ELSEVIER

Tribology International 34 (2001) 653–682

TRIBOLOGY INTERNATIONAL

www.elsevier.com/locate/triboint

A review of the experimental techniques for the measurement of heat and temperatures generated in some manufacturing processes and tribology

R. Komanduri *, Z.B. Hou

Mechanical and Aerospace Engineering, Oklahoma State University, Stillwater, OK 74078, USA

Received 27 September 2000; received in revised form 20 June 2001; accepted 19 July 2001

Abstract

Several techniques have been developed over time for the measurement of heat and the temperatures generated in various manufacturing processes and tribological applications. They include: (1) thermocouples — the embedded thermocouple and the dynamic thermocouple (or the chip–tool thermocouple in the case of cutting), (2) infra-red photography; (3) infrared optical pyrometers, (4) thermal paints, (5) materials of known melting temperatures, either in the powder form, or, as a thin film, and (6) change in microstructure with temperature in the case of high-speed steel tools, to name some. Each technique has its own advantages and disadvantages. The appropriate technique for a given thermal problem depends on the situation under consideration, such as the ease of accessibility, spot size, dynamics of the situation, accuracy needed, cost of instrumentation, advancements in technology. In this paper, these techniques are briefly reviewed with pros and cons on their application for a given situation.

1. Introduction

In many manufacturing processes as well as in tribological applications, it is desirable and often times necessary to have some knowledge on the amount of heat generated and consequent temperature rise (both maximum and average) as well as its distribution in the conduction medium. For example, the maximum temperature on the tool rake face or the clearance face of a cutting tool will determine the life of a cutting tool. Optimum cutting conditions used, especially the cutting speed, depend on this as well as on the characteristics of the cutting tool material with respect to the work material. Similarly, subsurface deformation, metallurgical structural alterations in the machined surface, and residual stresses in the finished part depend on the maximum temperature, the temperature gradient, and the rate of cooling of the part. The development of new tool materials as well as the advancement of machining technology will depend to a large extent on the knowledge and limitations of the cutting temperatures on the tool material, for they influence the life and performance of the tool. Similarly, the selection of an appropriate boundary lubricant in a gearbox depends on the flash temperatures generated and the stability of the fluid.

In tribological applications, as in the case of two contacting bodies in sliding contact, high surface temperatures (or flash temperatures), according to Kennedy [1], can have the following consequences: (1) surface melting, (2) oxidation and wear, (3) thermoelastic instabilities in the contact zone, (4) deterioration of solid or boundary lubrication films resulting in the exposure of the virgin surfaces and subsequent adhesion and galling between mating surfaces, (5) ignition of one of the contacting bodies, and (6) thermo–mechanical failure, such as thermal cracking, or warping.

Most of the energy expended in plastic deformation and friction in metal cutting and metal forming is converted into heat [2]. It is possible to estimate the heat generated in various manufacturing processes and tribological situations either by calorimetric methods or by measuring the forces generated. However, the measurement of temperature generally is not such a simple and

* Corresponding author. Tel.: +1-405-744-5900; fax: +1-405-744-7873.

E-mail address: ranga@ceat.okstate.edu (R. Komanduri).

0301-679X/01/$ - see front matter
PII: S0301-679X(01)00068-8

straightforward matter. The heat partition between two bodies which are in contact and moving with respect to the other is also a difficult problem.

Several techniques have been developed over time for the measurement of temperature in various manufacturing processes and tribological applications. They include: (1) thermocouples — the embedded thermocouple and the dynamic thermocouple (or the chip–tool thermocouple in the case of cutting), (2) infra-red photography; (3) optical infrared radiation pyrometers, (4) thermal paints, (5) materials of known melting temperatures, either in the powder form, or, as a thin film, and (6) change in microstructure with temperature in the case of high-speed steel tools, to name some. Several detailed reviews are available in the literature and may be referred to for further details. These include a brief review by Lenz [3] on the temperatures in metal cutting, by Barrow [4] on experimental techniques for assessing cutting temperatures, and by Kennedy [5] on the surface temperature measurement in tribology. In the following, calorimetric methods of estimation of the heat generated in machining will be briefly reviewed first, followed by various techniques used for the measurements of temperatures in machining, grinding, and tribological applications.

2. Determination of the heat generation

2.1. Calorimetric methods

The heat generated in cutting was one of the first and the foremost topics investigated in machining. Pioneering work in this area was due to Benjamin Thompson (Count Rumford) [6] who in 1798 investigated the heat generated in the boring of a cannon and developed the concept of mechanical equivalent of heat, the exact relationship of which was established by Joule [7] some 50 years later. Rumford used the calorimetric method to estimate the heat generated in the boring operation. He was fascinated by the heat acquired by a brass cannon in a short time during boring and with the still more intense heat (higher temperatures), much greater than boiling water, of the metallic chips. He was quite curious as to how this amount of heat was produced in a purely mechanical operation, such as boring, without the aid of any of the five elements of nature, especially fire. Rumford conducted a systematic investigation to inquire into the source of heat excited by friction between a blunt boring bar rubbing against the bottom of the bore of a cylinder of a cannon. Figure 1 is a schematic of the calorimetric setup used by Count Rumford to determine the heat generated in the boring of a cannon [6].

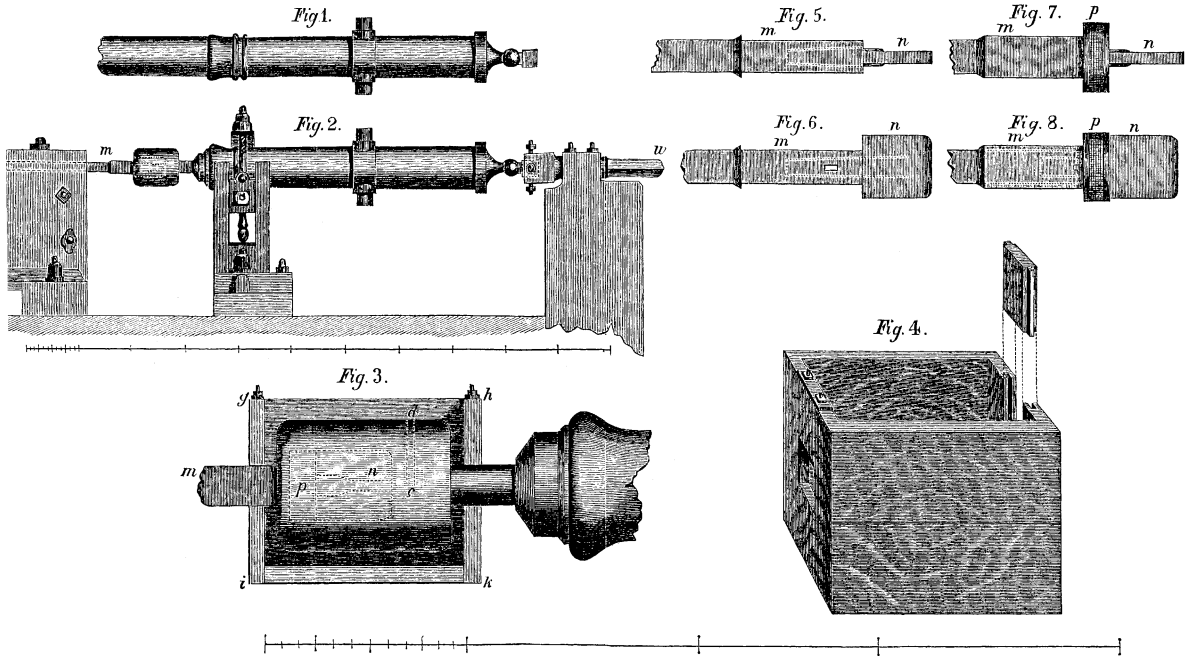

Fig. 1. Schematic of the calorimetric setup used to determine the heat generated in the boring of a cannon; after Rumford [6]. On the top is the cannon in the as-received state at the foundry. Below it is the experimental set-up used. The bottom figure is higher magnification of the calorimetric set-up showing the iron bar to the end of which a blunt boring tool is fixed, which is forced against the bottom of the bore in a cannon.

Rumford states in his communication to the Royal Society [6] and we quote: “the more I meditated on this phenomena, the more they appeared to me to be curious and interesting. A thorough investigation of them seemed even to bid fair to give further insight into the hidden nature of heat; and to enable us to form some reasonable conjectures respecting the existence, or the non-existence of an *igneous fluid*, a subject on which the opinions of the philosophers have in all ages been much divided”.

Joule, credited with the mechanical equivalent of heat (J) in his classical paper [7] that appeared some 50 years after the publication of Rumford’s paper, summed up Rumford’s contributions thus: “that justly celebrated natural philosopher demonstrated by his ingenious experiments that the very great quantity of heat excited by the boring of a cannon could not be ascribed to a change taking place in the calorific capacity of the metal; and he, therefore, concluded that the motion of the borer was communicated to its particles of metal, thus producing the phenomena of heat”. Joule continues, “one of the most important parts (of Count Rumford’s paper), though one to which little attention has hitherto been paid, is that in which he makes an estimation of the quantity of mechanical force required to produce a certain amount of heat. The power of a horse was estimated by Watt as 33,000 ft-lb (44.72 kJ), which according to Count Rumford’s experiment, will be equivalent to 26.58 lb (12.05 kg) of water raised by 180°F (82.2°C). Hence, the heat required to raise one pound of water by 1°F will be equivalent to the force represented by 1034 ft-lb (1.4 kJ). This result is not very different from that which I deduced from my own experiments related in this paper, viz. 772 ft-lb (1.05 kJ)”. “It appears to me”, Joule quoting Rumford, “extremely difficult, if not impossible, to form any distinct idea of anything, capable of being excited and communicated, in the manner that heat was excited and communicated in these experiments, except it be motion.”

This masterpiece study not only probed the source of frictional heat generated in the boring of a cannon but also the very nature of heat during an era when heat was considered as either an *igneous fluid* or a material property; it also provided a research methodology par excellence. Subsequently, F.W. Taylor [8] in 1906 recognized the importance of heat in accelerating tool wear and developed an empirical relationship between the cutting speed (consequently the tool temperature) and the tool life which is still in use today. He also developed a more heat resistant material, termed the high speed steel (HSS), which is still used extensively in machining not at high cutting speeds but towards the lower end of the cutting speed spectrum.

Practically all the energy expended in metal cutting is transformed into heat which manifests itself in varying amounts in the tool, workpiece, and chips. Heat gener-

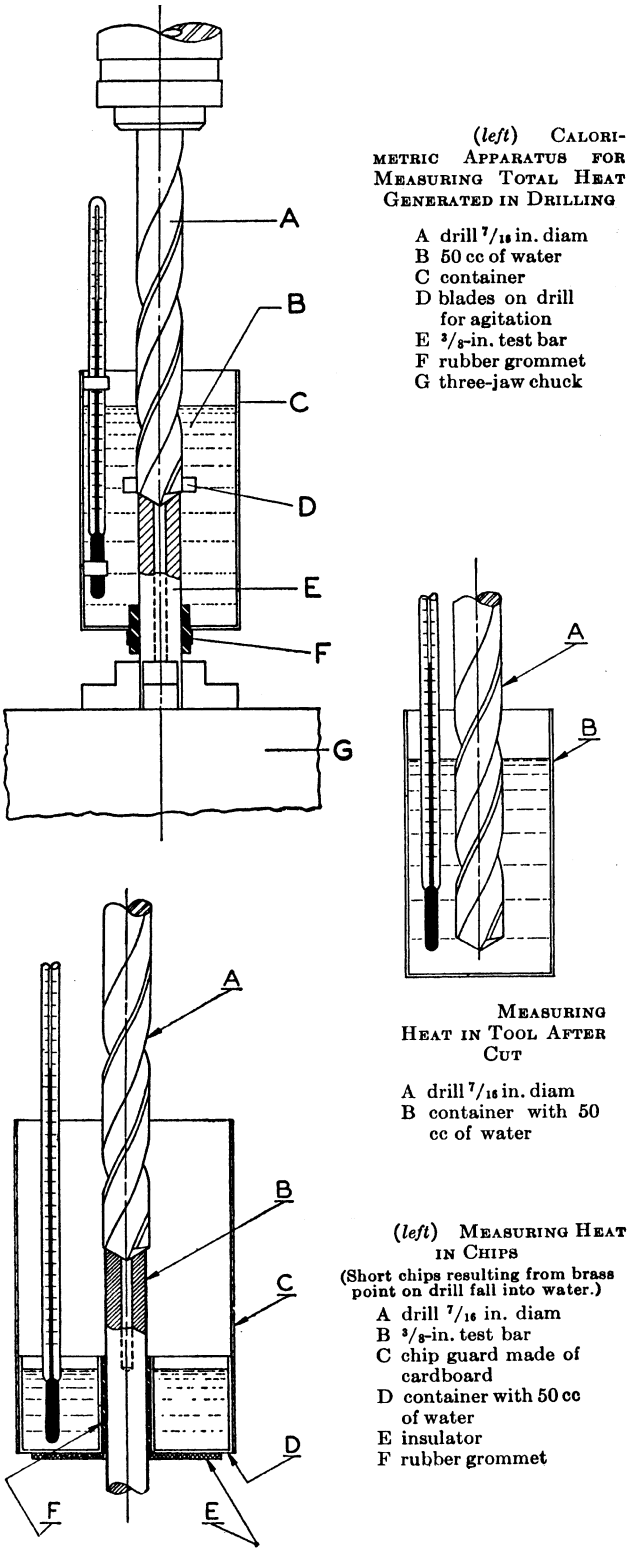

Fig. 2. Calorimetric set-up for the estimation of the total heat generated as well as the heat partition in the workpiece, tool, and the chips in drilling. (a) Total heat generated in drilling; (b) heat in the tool; (c) heat in the chips; after Schmidt and Roubik [10].

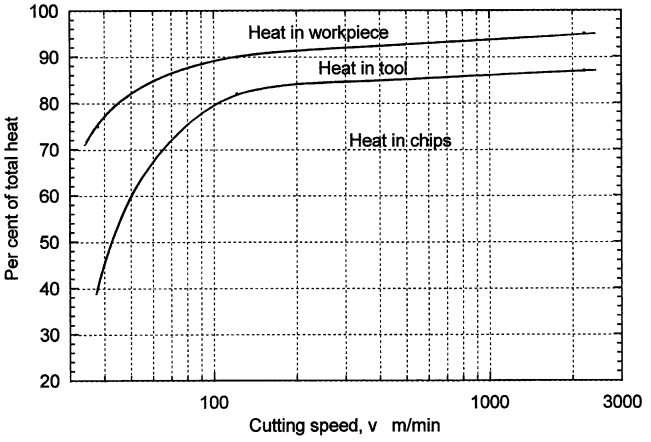

Fig. 3. Typical distribution of heat in the workpiece, the tool, and the chips with cutting speed; after Schmidt and Roubik [10].

ated in cutting can be determined rather accurately with a calorimeter. The measurements, thus obtained, permits computation of work, power, forces, average temperature of the chip, etc., as elegantly shown by Schmidt et al. [9] in 1945. They also showed a good agreement between the calorimetric measurements and the power data obtained from torque and thrust measurements.

Distribution of the heat generated in drilling was investigated by Schmidt and Roubik [10]. The objective of that study was to determine the amount of heat which conducts into the workpiece, the chip, and the tool (drill) at different cutting conditions, namely, the cutting speed and the in-feed rate. They used an ingenious method of determining the partition of heat generated in cutting between the tool, the workpiece, and the chip. Three different calorimetric setups were used for determining (i) the total heat generated in drilling, (ii) heat in the tool after the cut, and (iii) heat in the chips. Figure 2(a) to (c) show schematics of the drilling set-ups used for the calorimetric determination of the heat generated as well as its partition into the workpiece, tool, and chips, after Schmidt and Roubik [10]. The total heat was measured by performing the drilling operation with the workpiece, the chips, and the tool submerged in water [Fig. 2(a)]. The heat in the tool was determined by cutting an identical test bar dry and dropping the tool into the calorimeter immediately upon the completion of cutting [Fig. 2(b)]. Heat in the chips was obtained by noting the temperature rise of the calorimeter and water into which only chips were permitted to fall. Figure 3 is a typical distribution of heat in the workpiece, the tool, and the chips [10]. Schmidt and Roubik [10] showed quantitatively for the first time that much of the heat generated in cutting was carried out by the chips (~70–80%) with ~10% entering the workpiece, and the remainder into the tool. Since the workpiece is usually of a larger mass than the tool, its temperature rise due to cutting will be low, while the heat in the tool is, of necessity, concentrated in a small region near the cutting edge and hence can reach high temperatures.

Sato [11] and subsequently Malkin [12] and Brecker [13] conducted a similar calorimetric study of the grinding process and showed that much of the heat generated in grinding is conducted into the workpiece (~80%) and only a small fraction is carried away by the chips and the abrasive grains of the grinding wheel. This was attributed, subsequently, by Hahn [14], Shaw [15], Komanduri [16] amongst others, to the fact that most abrasive grains on the average present a high negative rake angle (approximately -55 to $-65°$) and the wear of the abrasives plays an important role in the heat partition.

In the following, various techniques used for the determination of temperature and its distribution will be briefly covered.

Table 1
Standard thermocouple types [17]

SLD[a]	Popular name	Materials (color code) (positive material appears first)	Typical temperature range	Seebeck coefficient at 100°C (212°F), μV/°C
S	–	Platinum–10% rhodium vs. platinum	−50 to 1767°C	7.3
R	–	Platinum–13% rhodium vs. platinum	−50 to 1767°C	7.5
B	–	Platinum–30% rhodium vs. platinum–6% rhodium	0 to 1820°C	0.9
T	Copper–constantan	Copper (blue) vs. a copper–nickel alloy (red)	−270 to 400°C	46.8
J	Iron–constantan	Iron (white) vs. a slightly different copper–nickel alloy (red)	−210 to 760°C	54.4
E	Chromel–constantan	Nickel–chromium alloy (purple) vs. a copper–nickel alloy (red)	−270 to 1000°C	67.5
K	Chromel–Alumel	Nickel–chromium alloy (yellow) vs. nickel–aluminium alloy (red)	−270 to 1372°C	41.4
N	Nicrosil–Nisil	Nickel–chromium–silicon alloy (orange) vs. Nickel–chromium–magnesium alloy (red)	−270 to 1300°C	29.6

[a] Standard letter designation.

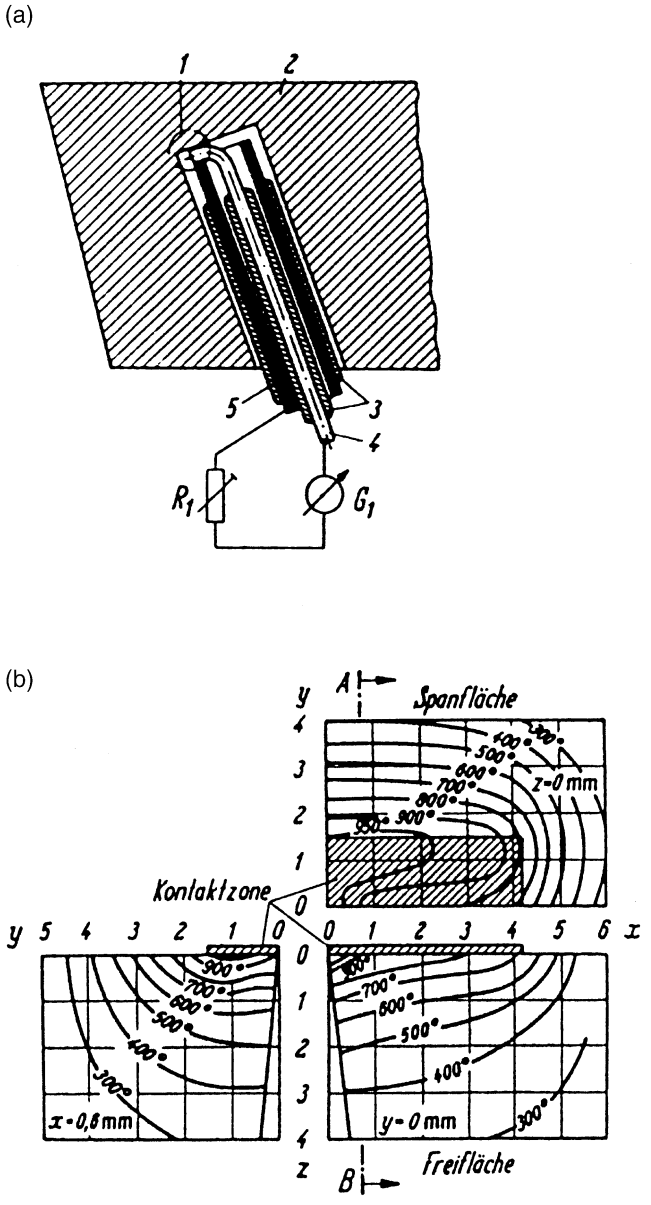

Fig. 4. (a) Schematic of the thermocouple inserted into the tool; (b) isotherms of the temperatures (°C) when machining a 30 Mn 4 steel at a cutting speed of 1.583 m/s^{-1} with a carbide tool; after Kusters [20].

3. Techniques for temperature measurement

3.1. Thermocouple method

The measurement of temperature by a thermocouple works on the principle that when two dissimilar metals are joined together to form two junctions and if these junctions were maintained at two different temperatures (the hot junction and the cold junction), an electromotive force (emf) exists across the two junctions. The emf generated is a function of the materials used for the thermocouple as well as the temperatures at the junctions. Table 1 gives the temperature ranges for eight standard thermocouples [17]. Thermocouples containing noble metals, such as platinum, and platinum–rhodium combinations (Types B, R, and S) are called noble metal thermocouples, while the rest (Types E, J, K, N, and T) are called base metal thermocouples.

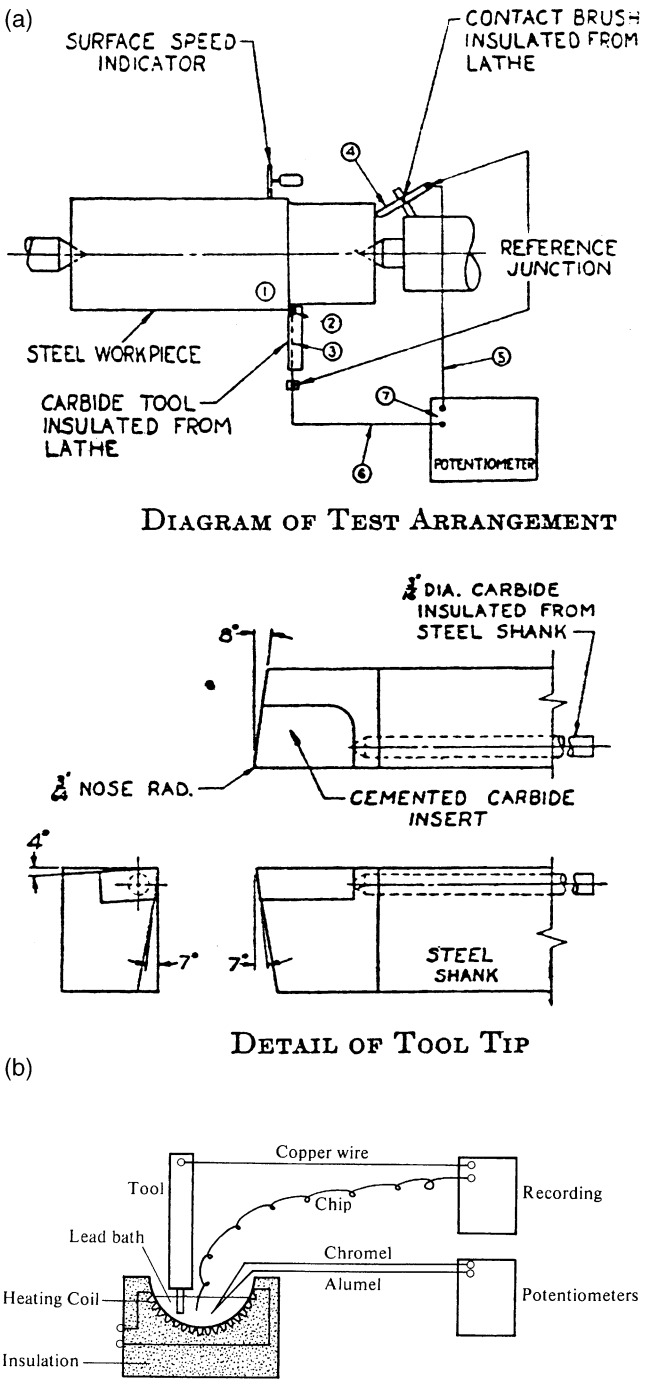

Fig. 5. (a) Schematic of the experimental set-up (with details of the tool tip) used for determining the tool temperatures using the chip–tool thermocouple technique; after Trigger [25]; (b) a schematic of the experimental set-up used for the calibration of the tool–chip thermocouple; after Shaw, [27].

The three laws of the thermoelectricity (the Seebeck effect) which are applicable to thermocouples are given by the following (Shaw, [27]):

1. The emf in a thermoelectric circuit depends only on the difference in temperature between the hot junction and the cold junction, and is independent of the gradients in the parts making up the system.
2. The emf generated is independent of the size and resistance of the conductors.
3. If the junction of two metals is at a uniform temperature, the emf generated is not affected by a third metal, which is at the same temperature, used to make the junction between the first two.

Advantages of thermocouples include the following: (1) simple in construction, (2) ease of remote measurement, (3) flexibility in construction, (4) simplicity in operation and signal processing, and (5) low cost.

There are two types of thermocouples, namely, the embedded thermocouples and the dynamic thermocouples (or tool–work thermocouples). In the following, these two types will be briefly discussed.

3.1.1. Embedded thermocouples

Embedded thermocouples were one of the earliest thermocouples used for the estimation of temperatures in various manufacturing and tribological applications. In order to use this technique, say for example, in machining, a number of fine deep holes have to be made in the stationary part, namely the cutting tool, and the thermocouples are inserted in different locations in the interior of the tool, with some of them as close to the surface as possible. Since, multiple holes can alter the heat conduction into the tools as well as limit the strength of the tool, only a limited number of holes (generally only one) can be drilled in any given tool. As a consequence, a large number of tools with the thermocouple hole drilled at different locations in each tool to cover the cross-section of the tool is required. Drilling of these holes in hard tools by conventional machining is at best difficult, if not impossible and expensive. These days, non-traditional machining techniques, such as EDM, or laser drilling are generally used to make these holes in view of the high hardness of the tools and relative ease of drilling holes by these techniques. However, this can be rather costly, especially when multiple holes have to be drilled to determine the temperature distribution. From the measurements of local temperatures at various points in the tool cross-section, the temperature field (and consequently the temperature isotherms) is obtained and the temperature on the surface is found by extrapolation.

Rall and Giedt [18] used an instrumented tool holder to determine the average temperature at the chip–tool interface. They used two HSS tools (with 0° and 15° back rake angles) instrumented with thermocouples located in the tool at selected distances from the cutting edges. Extrapolation of the temperature measurements to the center of the tool–chip contact area gave values of

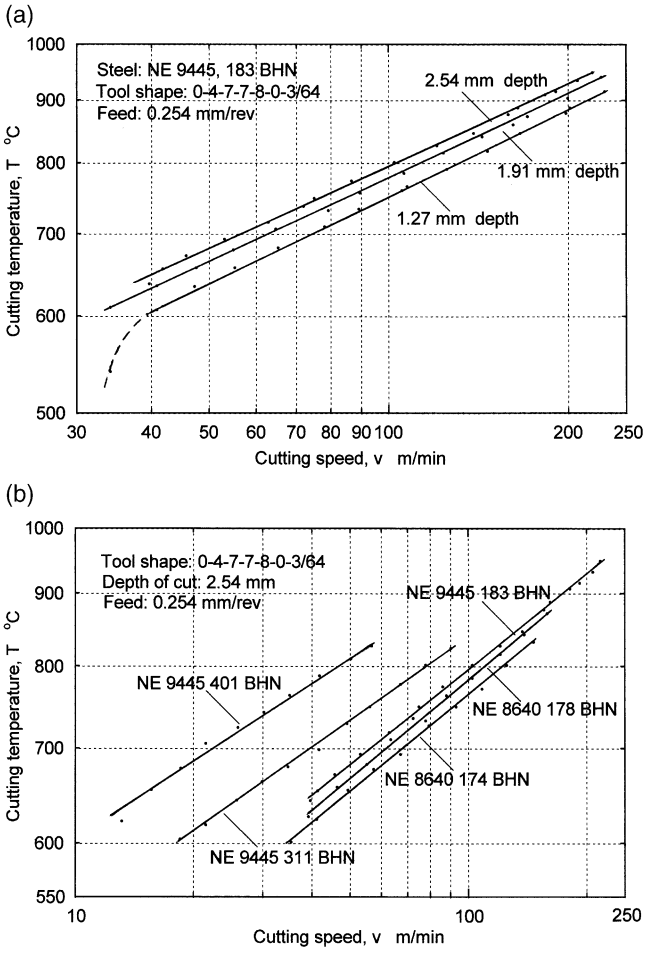

Fig. 6. Variation of cutting temperatures with cutting speed (a) at different depths of cut and (b) for NE 9445 steel at different hardness values from 174 BHN to 401 BHN; after Trigger [26].

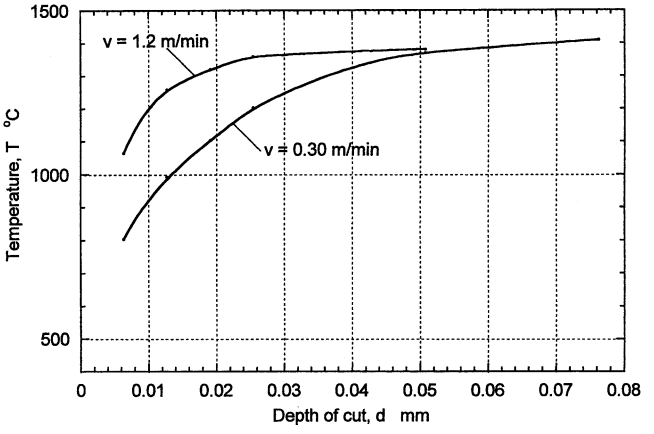

Fig. 7. Variation of chip–grit interface temperature with depth of cut for two work speeds [v=0.005 and 0.020 ms^{-1} (1 and 4 fpm)]; after Outwater and Shaw [28].

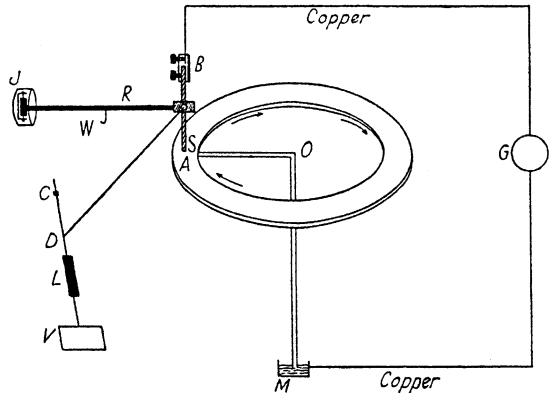

Fig. 8. Schematic of the experimental set-up used for measuring the surface temperature in sliding; after Bowden and Ridler [29].

the average tool–chip interface temperatures that are reported to agree reasonably well with the results of the other investigators [19].

This technique involving extremely difficult, very precise, and time consuming measurements was employed by Kusters [20] to determine the entire temperature field (a total of more than 400 points). Thermocouple holes of 0.32 mm were drilled by EDM in cemented carbide tools and a chrome–nickel thermocouple of 0.07 mm was inserted inside a nickel tube of 0.2 mm outer diameter and 0.14 mm inner diameter with proper electrical insulation in the drilled holes. Figure 4(a) is a schematic of a thermocouple inserted in the tool, after Kusters [20]. The temperature distribution in the tool was measured to within a distance of 0.2 mm from the surface of the tool. From the measured isotherms, a graphical extrapolation was made to establish the isotherms on the surface. Figure 4(b) shows the isotherms of the temperatures when machining a 30 Mn 4 steel at a cutting speed of 1.58 ms^{-1} with a carbide tool. Qureshi and Koenigsberger [21] used a similar method by inserting the thermocouple in the tool but instead of using a large number of tools with the thermocouples at different locations, as in the case of Kusters [20], they ground the rake and clearance faces of the tool progressively to obtain the temperature distribution in the tool with only one initial hole in the tool for the thermocouple. They found the maximum cutting temperature was not at the cutting edge but at some distance away from it, the point of maximum temperature moving towards the end of the tool–chip interface contact with increase in speed and/or feed.

The limitations of the embedded thermocouples include the following: (1) plotting of the temperature isotherms using embedded thermocouples in the tool can be an extremely tedious procedure, (2) the use of embedded thermocouples close to the chip–tool contact region is difficult and generally considered unsatisfactory as their placement can interfere with the flow of heat, (3) the technique is difficult to implement as it involves the use

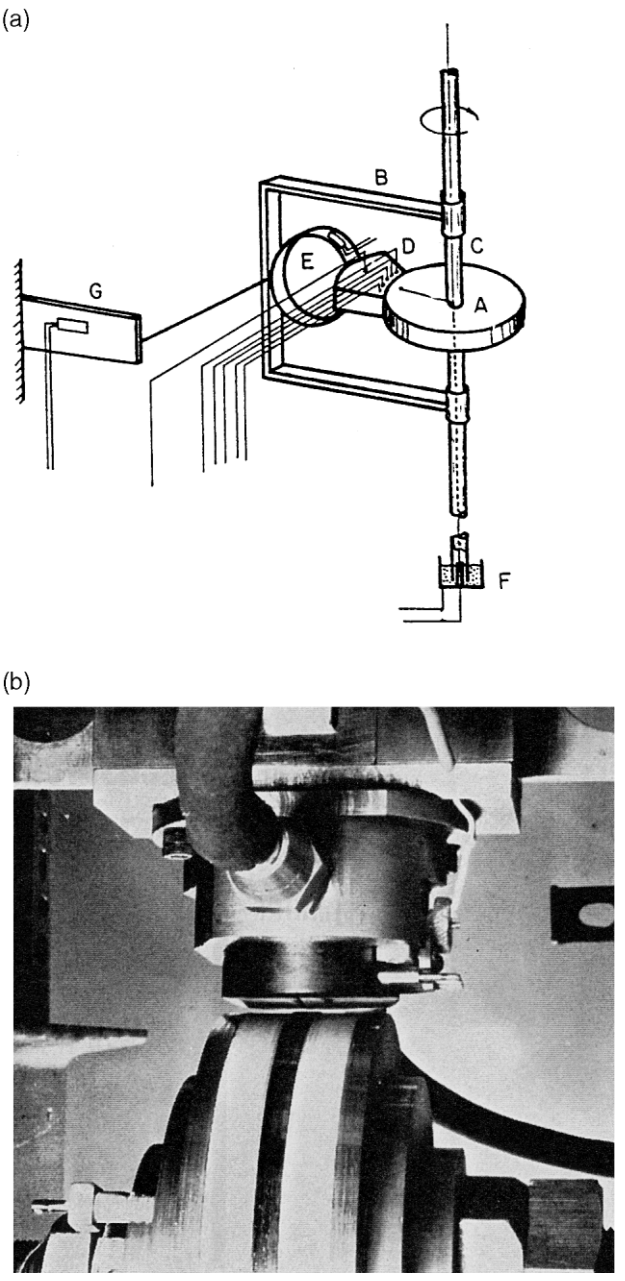

Fig. 9. (a) Schematic and (b) a close-up photograph of the test section to investigate the temperatures generated at the interface of two bodies in sliding contact; after Ling and Simkins [33].

of fine holes (to locate the thermocouples), in many cases, in hard and difficult-to-machine (or drill) materials, such as ceramics, cemented carbides, and hardened HSS tools, (4) the temperature gradients at the surface are rather steep and in many situations have to be estimated as it would be difficult to locate two thermocouples very close to each other, and (5) thermocouples have limited transient response due to their mass and distance from the points of intimate contact.

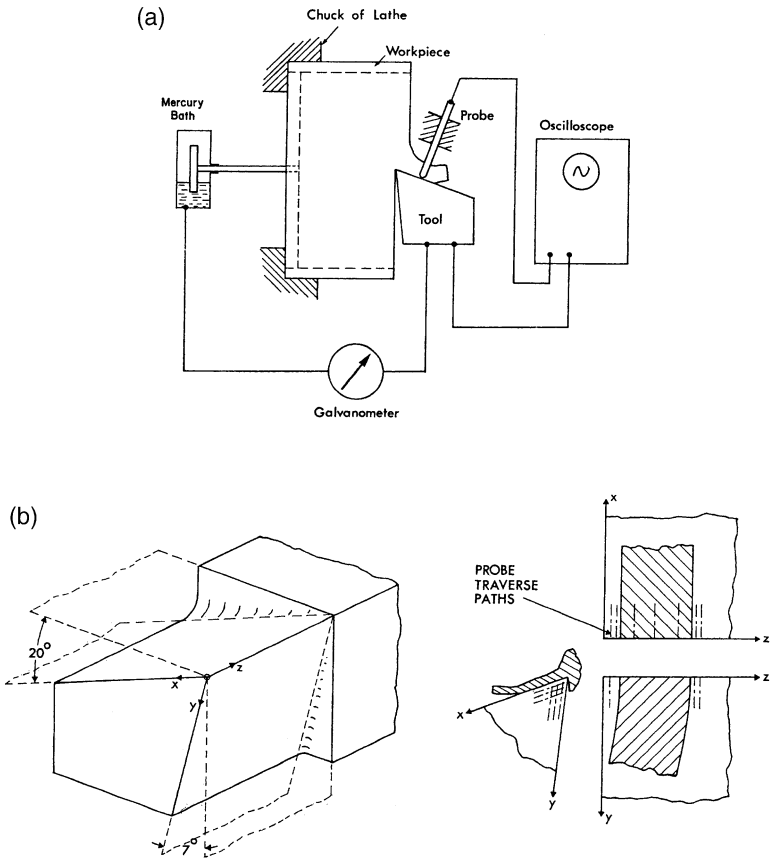

Fig. 10. (a) Schematic of the traverse probe thermocouple used in orthogonal machining; (b) traverses were made with the probe on all the three faces of the tool; after Arndt and Brown [37].

3.1.2. Dynamic thermocouples

Work on the dynamic thermocouple using the two bodies in relative motion as the two elements of the thermocouple was pioneered by Shore in the US [22] and by Gottwein in Germany [23] in 1925, and soon thereafter by Herbert in the UK [24], each developing this technique independently. This technique is often referred to as the Herbert–Gottwein technique in the tribology literature although it would be more appropriate to call it as the Shore–Gottwein–Herbert technique, since all three contributed simultaneously.

For investigating the chip–tool interface temperatures in cutting, it is not possible to use a pyrometer as the interface is not accessible to it. So, to address this problem, the tool was used as one element and the workpiece as the other element of the thermocouple, with the tool–work material interface forming the junction, and measured the thermoelectric emf. However, the tool support system as well as the workholding device have to be electrically insulated. The chip–tool thermocouple system was calibrated using the standard procedure involving heating them in a furnace at known temperatures and measuring the thermoelectric emf using a standard iron–constantan thermocouple. Herbert conducted several tests varying the cutting conditions, such as the speed and the depth of cut, as well as with different cutting fluids. His results showed that temperatures increased with increase in speed from 0.1 ms^{-1} (20 fpm) to 1 ms^{-1} (200 fpm). Similarly, temperatures were high when cutting dry, followed by cutting with an oil lubricant, and finally with water as the cutting fluid. Since water is the best conductor of heat among the three choices, it gave the lowest temperature, reinforcing water's ability as a good coolant.

Trigger [25,26] investigated the chip–tool interface temperatures using the Shore–Herbert–Gottwein thermocouple technique. This work differs from the earlier work in that cemented carbide tools (at higher cutting speeds) were used in machining steels instead of the high-speed steel (HSS) tools used earlier by Shore [22], Gottwein [23], and Herbert [24]. Also, to minimize wear, the HSS tools have to be used at low speeds to limit the tool temperature to 549°C (1000°F). With the carbide tools, the cutting speeds can be increased significantly and the resulting cutting temperatures can be in the range of 593–982°C (1100–1800°F). Another difference between Trigger's work and that of the earlier work [22–24] is that in the latter, both the elements of the chip–tool thermocouple comprise of iron–base alloys of similar basic lattice structure (steel work material and HSS

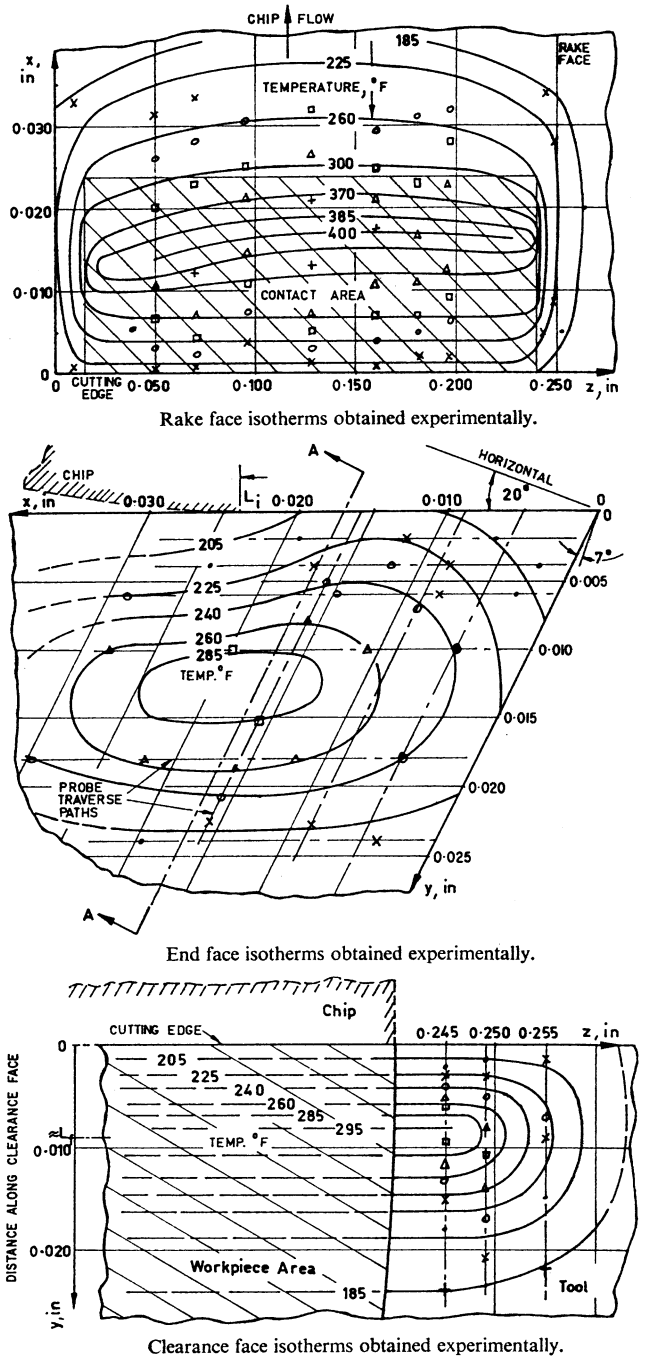

Fig. 11. Measured distribution of temperature (a) on the tool face, (b) end-face, and (c) clearance face of the tool; after Arndt and Brown [37].

tool material) — a factor which can influence the tendency of the chip to form a built-up edge on the tool and consequently cause erratic results. The dissimilar tool–work materials used in Trigger's investigations [25,26] can eliminate this factor and hence reduce the uncertainty. Also, the dissimilar material provides higher thermoelectric current thus increasing the accuracy of measurement. The *average chip–tool interface temperature* measured by this technique is designated as the *cutting temperature*.

Trigger [25] varied the cutting conditions, namely, the rake angle, the cutting speed, and the depth of cut as well as two different steel work materials of which the hardness of one was varied from 114–401 BHN. Figure 5(a) is a schematic of the chip–tool thermocouple set-up in turning, after Trigger [25]. The standard brazed carbide tool had a hole drilled in the shank through which a carbide rod 3, insulated from the shank is placed in contact with the carbide insert, 2, the assembly being electrically insulated from the tool post. A rotating wheel, 4 which is insulated from the lathe and immersed in a mercury bath provides the rotating contact. The chip–tool thermocouple was calibrated using a piece of the work material in contact with the tool and heating the combination in a furnace at known temperatures or in a molten bath of different materials of known temperatures. Figure 5(b) is a schematic of the experimental set-up used for the calibration of the tool–chip thermocouple [27]. A chromel–alumel thermocouple was used to measure the temperature between the work and the tool. Figure 6(a) and (b) show the variation of cutting temperatures with cutting speed at different depths of cut and for NE 9445 steel work material at different hardness values from 174 BHN to 401 BHN. It can be seen that the cutting temperature increases with increase in cutting speed, depth of cut, and hardness of the work material with the temperature ranging from 549°C–982°C (1000°F–1800°F). The relationship between the cutting speed and the tool temperature was approximated to a general equation of the form, $T=CV^n$ similar to the classical Taylor's tool life equation, $VT^n=C$. In a subsequent work, Trigger [26] used a steel grade triple carbide and compared the results obtained with the straight cemented tungsten carbide tool material used in the earlier study [25].

Outwater and Shaw [28] measured average grinding temperatures using the chip–tool thermocouple, in which the wheel–work interface constituted the hot junction. They selected a vitreous-bonded SiC grinding wheel having a relatively low contact resistance. While the thermoelectric power of a SiC wheel–steel combination is very much higher than that for a metal combination, the high impedance of the grinding wheel compared to a solid metal makes it difficult to measure the thermoelectric emf accurately. The advantage of the former is more than offset by the drawback of the latter. In addition, the measured temperature will be the time mean value for a number of cuts. Figure 7 shows the variation of temperature at the chip–abrasive grit interface with depth of cut for two work speeds [v=0.005 ms^{-1} and 0.02 ms^{-1} (1 and 4 fpm)] where each data point represents the mean of 10 independent readings. It can be seen that the mean temperatures reach values in excess of 1093°C (2000°F).

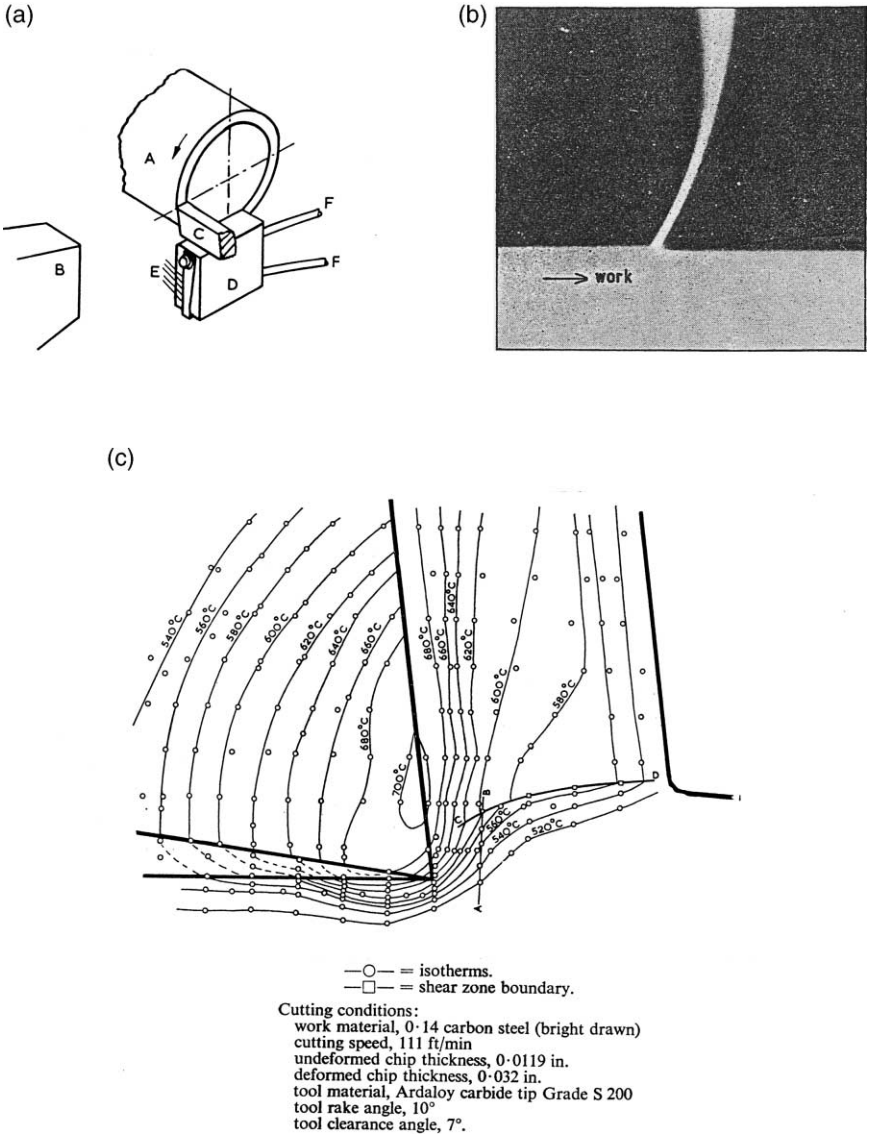

Fig. 12. (a) Schematic of the experimental arrangement used for IR measurements of temperatures generated in the cutting process; after Boothroyd [38]; (b) infrared photograph of the cutting process; after Boothroyd [39]; (c) temperature distribution in the shear zone, chip, and tool during orthogonal machining of AISI 1014 steel; after Boothroyd [38].

While the chip–tool thermocouple method is relatively simple to use, it has certain limitations [27]. First, it measures the mean temperature over the entire area between the chip and the tool including the wear land on the clearance face. Second, misleading results may be obtained if a built-up edge is formed because then dissimilar materials do not exist over the entire area. Third, there is a question whether static calibration is valid for a dynamic situation. Fourth, oxide layers formed on the carbide tools during machining may change the calibration of the tool–chip thermocouple. Fifth, for each tool–work material combination, separate calibration is needed. Sixth, a rotating contact as well as insulation of the workpiece system and the tool system are required.

In the field of tribology, Bowden and Ridler [29] determined the surface temperature of sliding metals using Shore–Gottwein–Herbert's dynamic thermocouple technique. Narrow cylinders of one metal were slid against discs of a second metal and the temperatures at the interface were determined by measuring the resulting thermal emf generated. Figure 8 is a schematic of the experimental set up used for measuring the surface temperature in sliding, after Bowden and Ridler [29]. One of the metals A is in the form of a flat annular ring rotating at a uniform velocity. A wire of the same metal A leads down the axis of rotation and is immersed in a mercury bath M to provide the rotating contact. This is connected by a copper wire to one terminal of a galvanometer G. The second metal B, which constitutes the other half of the thermocouple is in the form of a polished cylinder B which rests on the rotating ring at S. The metal B is connected by a copper wire to the other

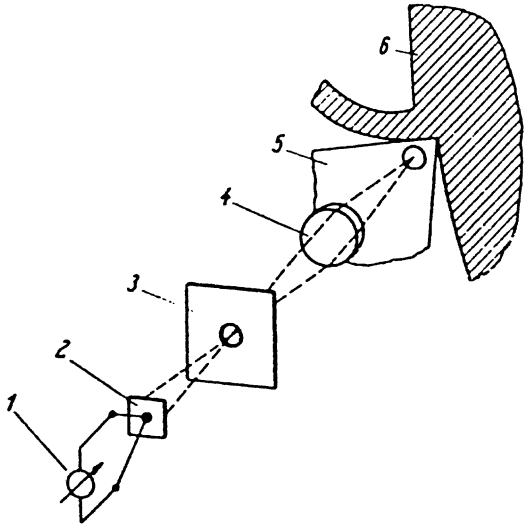

Fig. 13. Schematic of the total-radiation pyrometer used for determining the temperature distribution on accessible surfaces of the tool and the workpiece using an optical condenser; after Schwerd [41]. 1. Galvanometer; 2. thermocouple; 3. Shutter; 4. Optical condenser; 5. Tool; 6. Workpiece.

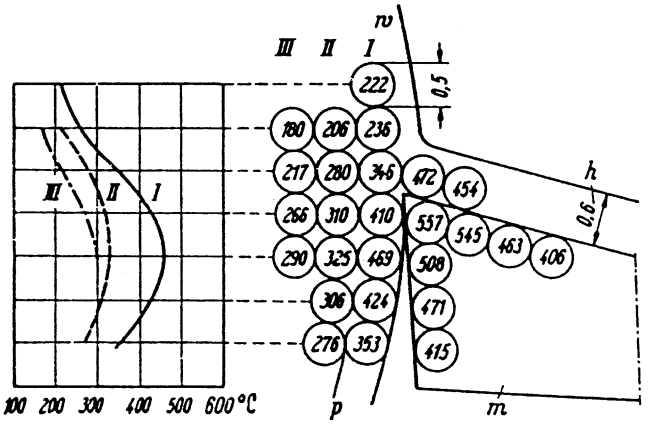

Fig. 14. Temperature distribution in cutting using a radiation pyrometer; after Kraemer [42].

terminal of the galvanometer. A cylinder B is attached to a light rigid arm AR which is carried on a gimbal J, so that the cylinder can move freely up and down, or to and fro. The required load is applied to the cylinder by adding weights to the arm at W. All the metal junctions except the sliding one at S are at room temperature.

The temperature reached in sliding depended upon the load, speed, coefficient of friction, and the thermal conductivity of the metals. As can be expected, when the surfaces were of the same metal, no emf is generated on sliding. When the surfaces were of different metals, the emf rose steadily as the load or the speed was increased and reached a definite maximum corresponding to the melting temperature of the fusible metal. They found the surface temperatures to vary inversely as the square root of the thermal conductivity in accordance with the theoretical thermal model they developed. They also found that the intense heat generated was confined to a thin layer at the surface of contact during sliding. They pointed out that the high surface temperatures can cause local volatilization and decomposition of the lubricant and is a cause for the breakdown of the boundary film. They also pointed out some of the limitations of the model, including the lack of knowledge on the size of the real area of contact (number and area of each contacting point) and the heat partition between the stationary and the rotating members in sliding contact.

Spurr [30] extended Bowden and Ridler's pioneering work in tribology. He conducted sliding friction tests to investigate the temperatures reached by a sliding thermocouple. Thermocouples as well as single wires were slid against discs of various metals (mild steel, brass, zinc, aluminum and copper) as well as polymethylmethacrylate (PMMA). He reported that the theory of Bowden and Ridler (which was further extended by Blok [31] and Jaeger [32]) overestimates the temperature reached when metals of low conductivity are used.

Ling and Simkins [33] experimentally investigated the temperatures generated at the interface of two bodies in sliding contact. They designed an apparatus that brought a rider and a slider into a continuous, sliding contact under controlled loads and speeds and instrumented it to measure the normal load, the frictional force, and the temperature of the rider. Figure 9(a) and (b) are a schematic and a close-up photograph of the test section, respectively, to investigate the temperatures generated at the interface of two bodies in sliding contact, after Ling and Simkins [33]. Provision was made to locate several thermocouples on the rider and the slider which are formed by using pointed rods of constantan pressed against the side of the specimen, thus forming a dynamic thermocouple. To complete the electrical circuit, a steel rod was brought into contact with the specimen in the same fashion. The temperature through the thickness of the rider was expected to be uniform. The leads of the slider were brought out through a pair of mercury bath-type contacts. The mercury receptacles were located at the lower end of the drive shaft. A hollow part of the shaft from the disk carried the necessary wiring. Calibration of the thermocouple was done in a furnace at various temperatures using constantan rods pressed against flat steel specimens. The temperature of the rider and the slider were computed using the appropriate heat conduction equations for a given configuration.

Furey [34] conducted a systematic study of the surface temperatures generated by friction in a sliding system using a stationary constantan ball 12.7 mm (0.5 in) diameter riding on a rotating steel cylinder of 44.45 mm (1.75 in) in diameter. The electrical connection to the rotating cylinder is established by means of a metal disc which is attached to the end of the rotating support shaft immersed in a mercury bath. The system was calibrated

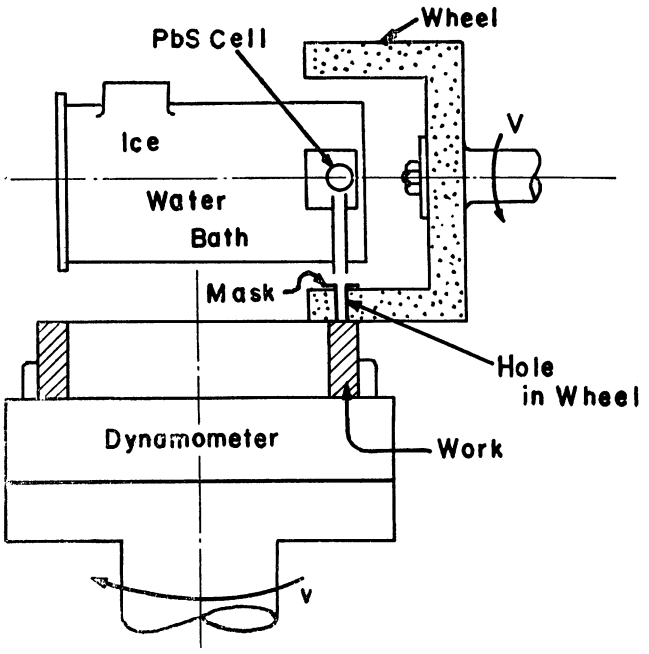

Fig. 15. Schematic of the surface grinding apparatus used for measuring the surface temperature of a freshly ground surface using a photoconducting PbS cell; after Mayer and Shaw [43].

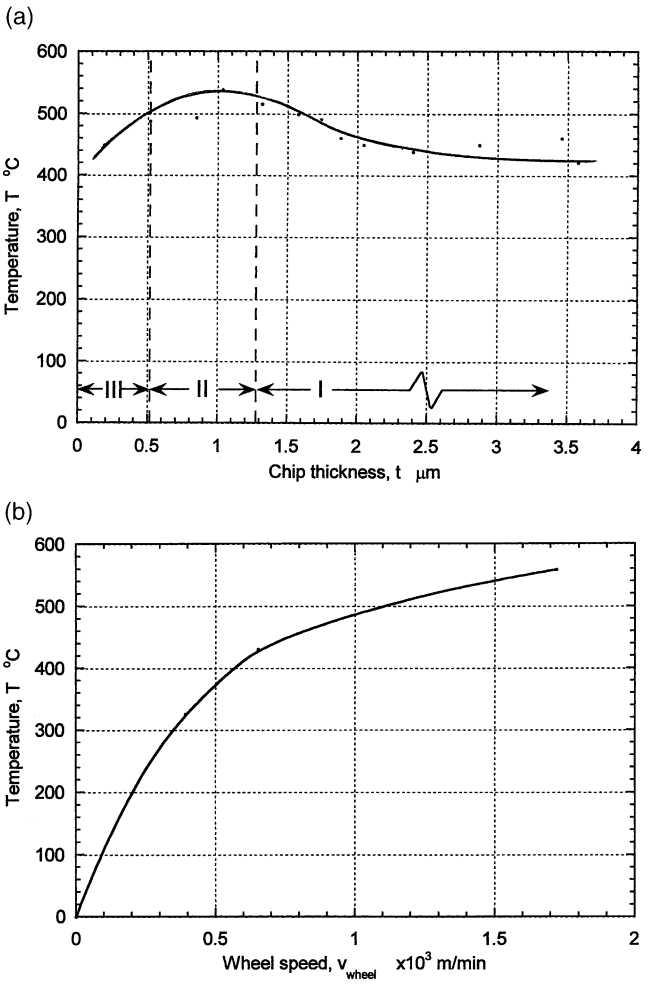

Fig. 16. (a) Variation of the observed surface temperature with chip thickness; (b) variation of surface temperatures with wheel speed; after Mayer and Shaw [43].

by maintaining the ball/cylinder junction at various known temperatures and measuring the thermo-electric emf. Using the principle of Shore–Herbert–Gottwein's dynamic thermocouple technique, Furey measured the average as well as the instantaneous temperatures generated. He investigated the effect of time, load [0.294–2.45 N (30–250 gm) corresponding to Hertzian contact pressures of 158.8–393 Mpa (28,400 to 57,000 psi)], and sliding speed of 0.14 to 2.24 ms^{-1} on the surface temperatures generated in pure sliding under dry (unlubricated) conditions. He found the average surface temperature to be independent of the running time and gross wear but increases significantly with speed and load. He also found the experimental results to be considerably lower than those predicted theoretically based on the work of Blok [31], Jaeger [32], and others. Plausible reasons for the lack of correlation were attributed to the fact that sliding surfaces are not plane and that the ball and the cylinder possess finite heat capacities. Dayson [35] subsequently attempted to explain the difference based on junction growth which occurs at the contacting asperities, the effect of which was not considered by Furey. Also, the effect of the distributed nature of the real area of contact over the apparent area of contact on the thermal contact resistance could also be an important consideration when comparing the experimental results with the theoretical analysis.

3.1.3. Thin film thermocouples

Recently, Tian et al. [36] used a thin film thermocouple (TFTC) for the measurement of contact temperature of sliding mechanical components. The thermocouples were made from thin films of vapor deposited copper and nickel. The junction of the thermocouple was ≈2 μm thick and 80–300 μm across. The response time of the thermocouple was extremely short (<≈1 μs) and it was reported that the presence of the thermocouple disturbed very little the heat flow from the sliding contact. To insulate the thermocouple electrically from the substrate and protect it during sliding, the thermocouple was sandwiched between a thin film of a hard, non-conductive ceramic (Al_2O_3). The thermocouple was applied to the measurement of a sliding surface in the case of (a) oscillatory dry sliding of a polymer pin on a flat surface, and (b) unidirectional dry sliding of a ring over the surface of a flat pin. It was found that the TFTC device, however, had to be calibrated individually because of slight variations in the thermoelectric power amongst the devices. The heat flow disturbance caused by the presence of the thin film thermocouple was investigated using a FEM package for surface temperature problems in sliding systems. It was found that there is very little

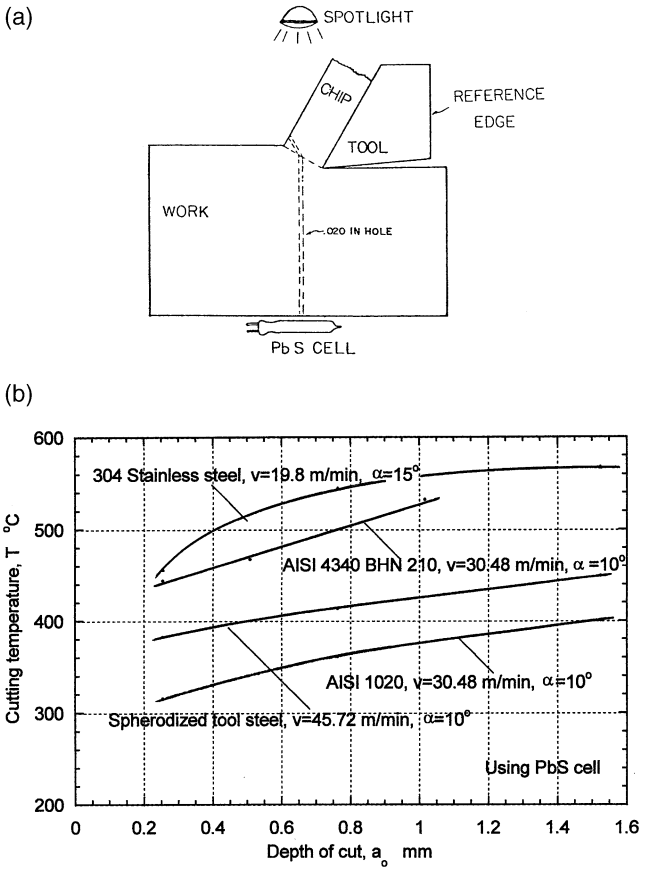

Fig. 17. (a) Schematic of the experimental set-up used for the determination of the shear plane temperature in cutting using a PbS cell; (b) variation of the shear plane temperature with depth of cut for different work materials and cutting speeds; after Reichenbach [44].

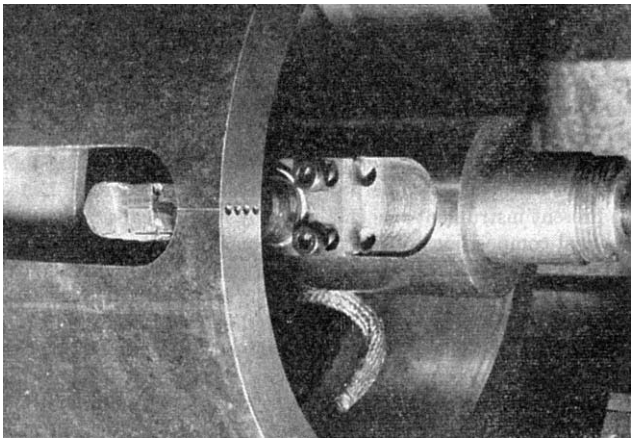

Fig. 18. Photograph of the experimental set-up used with an infrared detector for the determination of the temperature distribution at the tool–flank interface of a cutting tool in machining; after Chao et al. [45].

difference in the surface temperature with and without the TFTC under the contact zone. They verified the experimental results using the TFTC with some of the theoretical predictions.

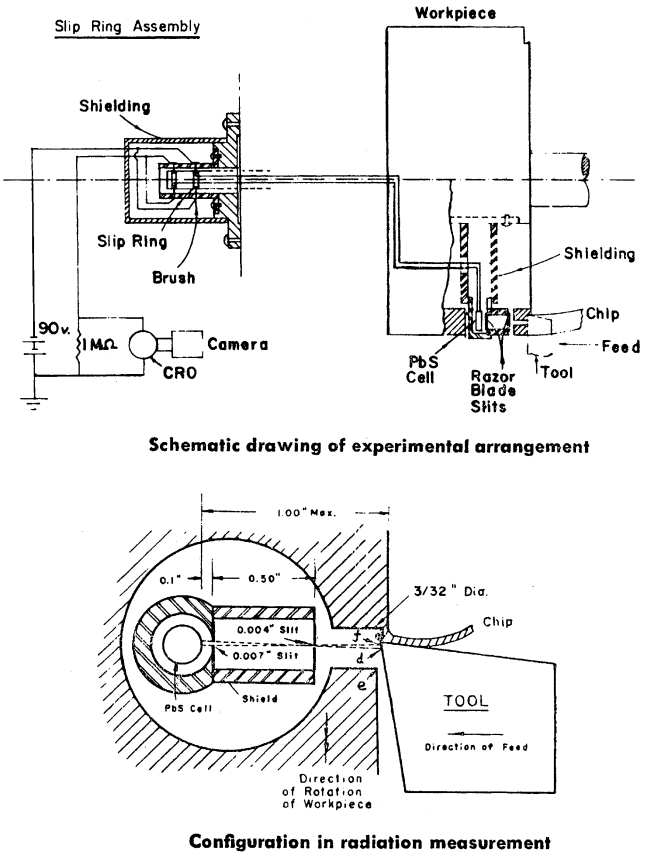

Fig. 19. (a) Schematic of the experimental arrangement and (b) the configuration of the sensor arrangement; after Chao et al. [45].

3.1.4. Traverse thermocouple technique

This technique is a modification of the chip–tool thermocouple in that the contact between the chip and the tool changes continuously as cutting proceeds. Arndt and Brown [37] developed a traverse thermocouple technique to obtain 3-dimensional tool temperature distributions on the end-, clearance-, and rake-face of the tool within the chip–tool interface area. The technique is based on the principle of forming a thermo–electric junction between the tool and a sharply pointed probe of dissimilar material (e.g. a high speed steel tool and a cemented carbide probe or vice versa). The probe was traversed continuously along an appropriate tool surface and the spot temperature is recorded. By varying the position of the moving probe, a continuous record of the temperature distribution relative to some edge of the tool can be obtained.

Figure 10(a) is a schematic of the traverse probe thermocouple, after Arndt and Brown [37]. The traverse probe moves over the tool face by a drive mechanism which incorporated a gear train, an adjustable swash plate and a motor. The probe and the tool were connected to form the hot junction of the thermoelectric circuit. Traverses were made with probe on all the three faces of the tool as shown in Fig. 10(b). Traverse within the chip–tool contact area was accomplished by splitting the

chip with a V-shaped tool located diagonally opposite to the cutting tool. A gap of at least 0.35 mm (0.014 in) in the chip was found to be necessary to accomplish this task. Figure 11(a)–(c) show the measured distribution of temperature on the tool face, end-face, and clearance face of the tool, respectively. An AISI 1011 steel work material, a high-speed steel tool, and a cutting speed used of 0.762 ms^{-1} (150 fpm) were used. Although this method is simple in concept, it is somewhat complicated to use. It can provide the isotherms of the temperature distribution as well as the location of the maximum temperature on the end-, clearance-, and rake-face of the tool.

3.2. Infrared photographic technique

Boothroyd [38,39] developed an infrared photographic technique to measure the temperature distribution in the shear zone and at the chip–tool interface in machining. The method involves photographing the workpiece, the chip, and the tool using an infrared (IR) sensitive photographic plate and measuring the optical density of the plate over the relevant field with a microdensitometer. A heated tapered strip, on which the temperature distribution was measured by means of a series of thermocouples, was mounted next to the tool and photographed simultaneously with the cutting process. The radiating surfaces of the workpiece, the tool, and the calibration furnace were coated with lamp black to ensure the same value of emissivity. Figure 12(a) is a schematic of the experimental arrangement used for the infrared measurement of temperatures generated in the cutting process and Fig. 12(b) is an infrared photograph of the cutting process. Figure 12(c) shows the temperature distribution in the shear zone, chip, and tool during orthogonal machining. Some of the limitations of this technique include the following: (1) the sensitivity of the infrared photographic plate was such that an exposure time of 10–15 s was required, (2) in order to obtain complete temperature patterns of the cutting process, it was necessary to preheat the workpiece between

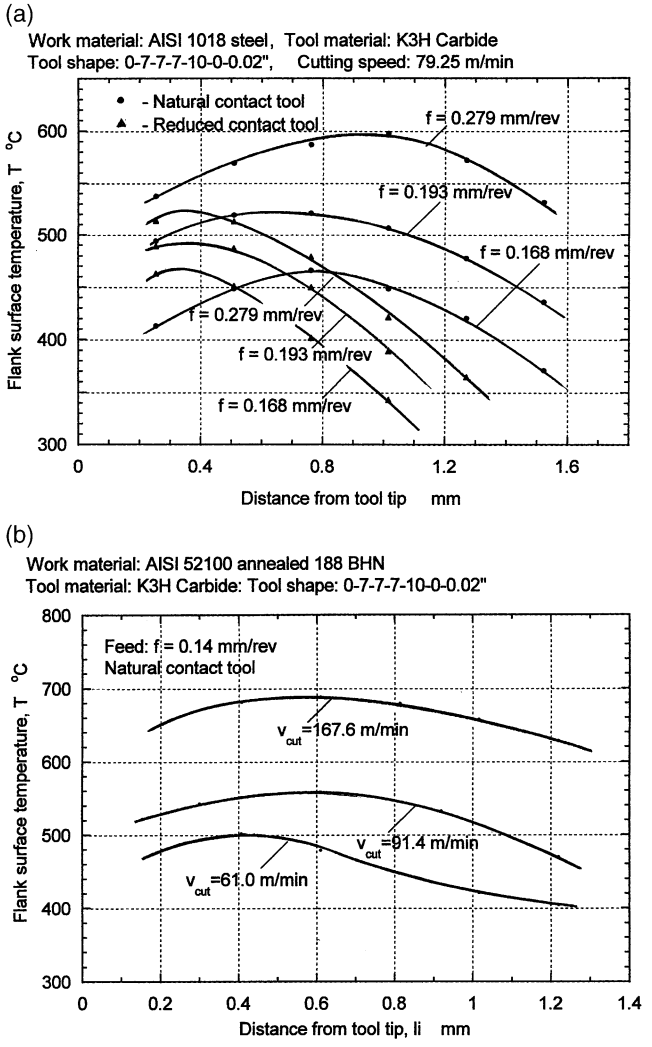

Fig. 20. Flank surface temperatures with the distance from the tool tip for (a) different feeds [and constant speed of 79.25 m/min (260 fpm)] when machining AISI 1018 steel work material and (b) at different speeds [and constant feed, 0.14 mm/rev (0.0055 ipr)] when machining AISI 52100 steel work material; after Chao et al. [45].

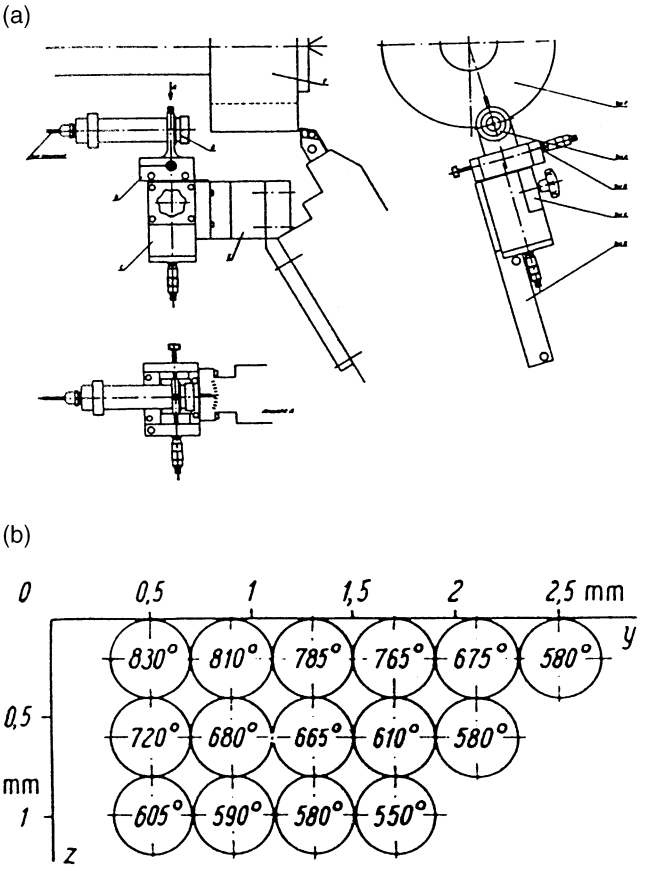

Fig. 21. (a) Experimental set-up used in the determination of the temperature distribution on the clearance face in longitudinal turning, using a radiation pyrometer; (b) isotherms of the temperatures (°C) for the clearance surface of the tool; after Lenz [47].

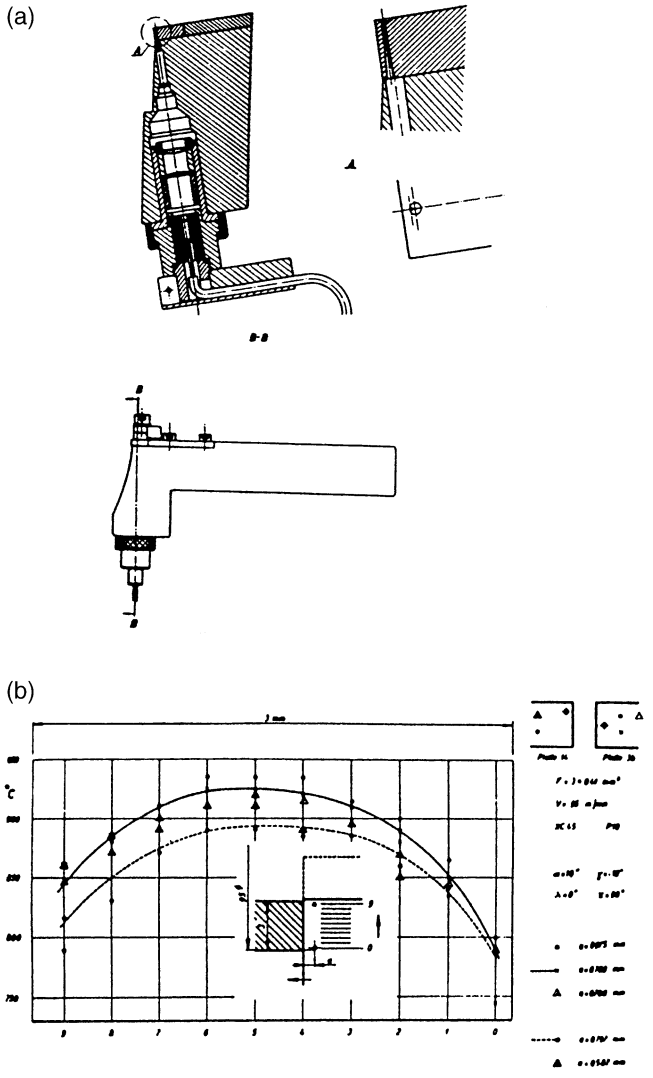

Fig. 22. (a) Schematic of the optical pyrometer mounted in the cutting tool to determine the temperature distribution at the chip–tool interface; (b) temperature distribution on the tool face when machining XC 45 steel with a P30 steel; after Lenz [47–49].

350–500°C and also to maintain cutting conditions which will not give a maximum temperature of more than 200°C above the initial workpiece temperature. The preheating of the workpiece was needed as the photographic film was not sensitive below this temperature. Consequently, the cutting speed must be kept relatively low.

Jeelani [40] subsequently conducted a similar study using IR photography to measure the temperature distribution in the machining of annealed 18% Ni Maraging steel in the cutting speed range of 0.406–0.813 ms^{-1} (80–160 fpm). He built a special light-tight enclosure around the lathe to eliminate stray light. He noted that the thermal sensitivity of the high speed IR film available had increased significantly since Boothroyd's [39], with the result that it was not necessary to preheat the work material. A 30 gauge chromel–alumel thermocouple was

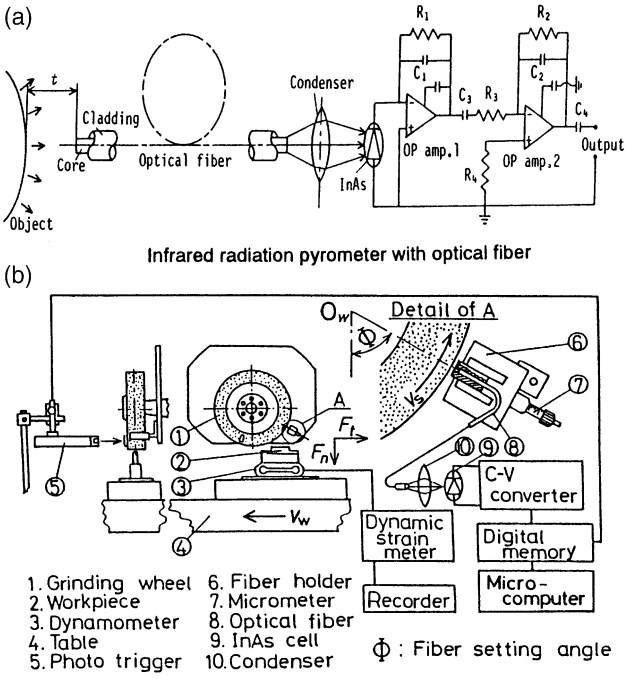

Fig. 23. (a) Schematic of the InAs radiation pyrometer system used and (b) the experimental grinding set-up; after Ueda et al. [52].

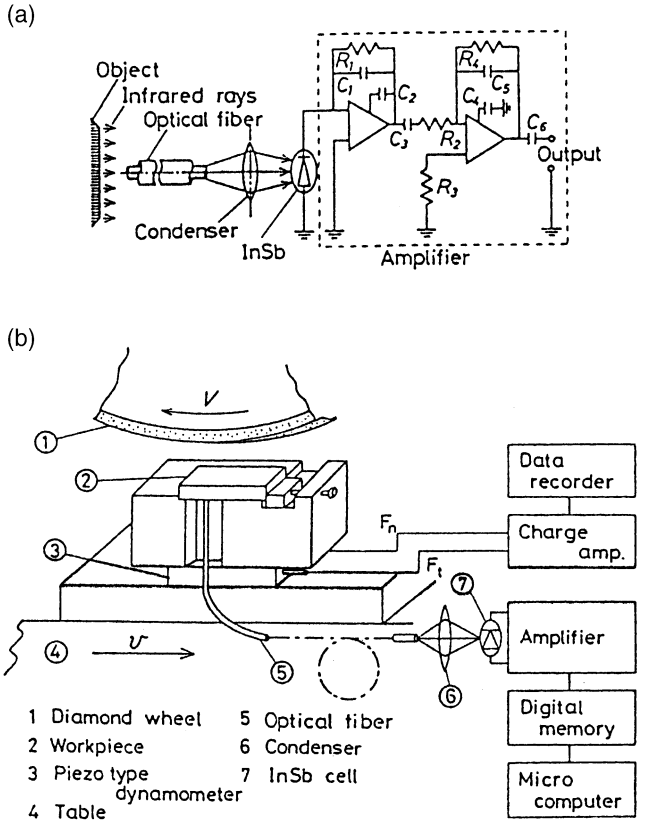

Fig. 24. Schematics of (a) the InSb pyrometer system and (b) the experimental set-up used; after Ueda et al. [54].

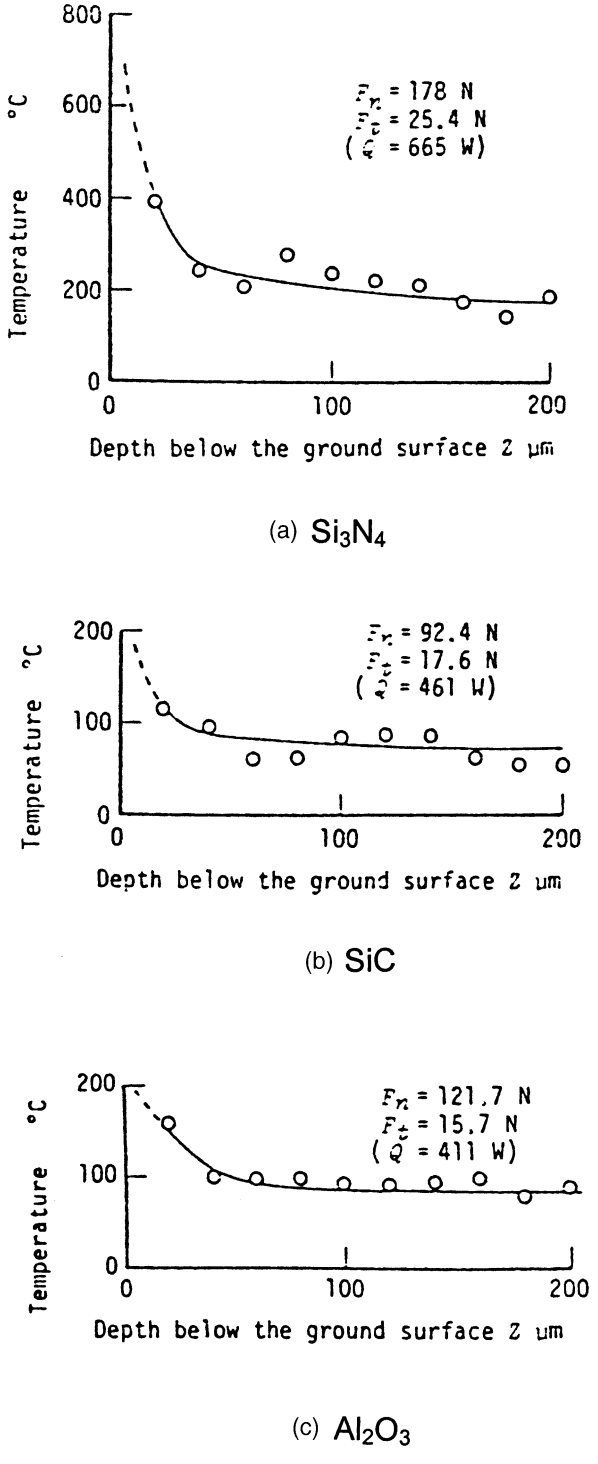

Fig. 25. Variation of the temperature with the depth below the ground surface for (a) Si_3N_4, (b) SiC, and (c) Al_2O_3; after Ueda et al. [54].

used for calibration. It was heated electrically and photographed at various temperatures. The workpiece, the cutting tool and the calibration bead were all coated with graphite to generate surfaces with similar emissivities. The IR film was developed and its density was read using a microdensitometer. He could not determine the temperature distribution below 400°C (750°F) as the IR film is insensitive to temperatures below this value. He reported that the temperature on the machined surface is quite high (555°C at a cutting speed of 0.813 ms^{-1}) and decreases with the depth beneath the surface. Also, the cutting temperature was found to increase with the increase in the wear or dullness of the tool.

3.3. Optical and infrared radiation pyrometers

Schwerd [41] designed a total-radiation pyrometer for determining the temperature distribution on accessible surfaces of the tool and the workpiece using an optical condenser (Fig. 13). Kraemer [42] further developed this technique and Fig. 14 shows the results of his work on the temperature distribution in cutting.

Mayer and Shaw [43] developed an ingenious apparatus for measuring the surface temperature of a freshly ground surface using a photoconducting PbS cell. Figure 15 is a schematic of the surface grinding apparatus used in this investigation. A 177.8 mm (7 in) white aluminum oxide grinding wheel was used for grinding an AISI 52100 steel work material. The workpiece was mounted on a dynamometer to measure the grinding forces. A small hole was drilled radially through the grinding wheel, as shown in Fig. 15. This enabled the PbS cell to sight upon the workpiece surface immediately after grinding. Since the resistance of the PbS cell is sensitive to changes in its ambient temperature as well as to the infrared radiation, the cell was kept at a constant temperature in an ice bath. The hole in the sighting tube was masked to provide a square opening of 1.59 mm (1/16 in) on a side. The PbS was calibrated by heating a piece of work material electrically and recording the temperature with a standard alumel–chromel thermocouple attached to the surface. Dry grinding tests were conducted at a wheel speed of 28.85 ms^{-1} (5680 fpm), but variable work speed [v=0.102–1.32 ms^{-1} (20–260 fpm)] and down feed 0.035–0.259 mm/min (0.0014–0.0102 ipm). Figure 16(a) shows the variation of the observed surface temperature with chip thickness. Grinding tests were also conducted at a constant value of chip thickness of 1.18 mμ (30 μin) but variable wheel speed (V=28.85 ms^{-1} (5680 fpm), 10.72 ms^{-1} (2110 fpm), and 6.5 ms^{-1} (1280 fpm). Figure 16(b) shows the variation of surface temperatures with wheel speed. Reasonable agreement of the experimental results with the analytical results were reported.

Reichenbach [44] used a radiation technique with a PbS cell to measure the temperatures in cutting. The cutting tests were conducted on a shaper. The PbS cell was arranged to sight through a small hole drilled in the workpiece sensing radiation from the shear plane and clearance face of the tool [Fig. 17(a)]. It was mounted facing a 0.508 mm (0.02 in) hole drilled in the workpiece. The PbS cell is essentially a resistance of ~0.5 mΩ whose resistance changes when exposed to radiation

in the infrared region (1–3 μm). This corresponds to the peak intensity of blackbody radiation distribution in the range of 260–1093°C (500–2000°F). Changes in the cell resistance were recorded as changes in the voltage on an oscilloscope. First, the cell sees the spotlight which was placed at a considerable distance to ensure parallel light rays. The spotlight had sufficient infrared radiation to activate the cell. As the tool advances into the cut, the shear plane arrives at the hole and closes it over, shutting off the light and producing a voltage change in the PbS cell. The PbS cell was located at different locations along the direction of cut so that the temperature distribution along the shear plane can be recorded. There were, however, some limitations in using this technique to determine the temperature distribution in the shear zone. For example, the minimum temperature which gave a useful reading was 232°C (~450°F). For the materials tested, the shear plane temperatures were mostly below this value except near the face of the tool. Therefore, Reichenbach could not obtain the temperature distribution along the entire length of the shear plane. Also, the fourth power radiation law gave such large variations in the readings that when the attenuation on the oscilloscope was set high enough to keep the maximum readings on scale, the low temperature regions could not be noticed. There was a 100 to 1 change in the reading when going from 260–549°C (500–1000°F). Figure 17(b) shows the variation of shear plane temperature with depth of cut for different work materials and cutting speeds.

Chao et al. [45] used an infrared detector for the determination of the temperature distribution at the tool–flank interface of a cutting tool in turning. A moving PbS photoconductive, infrared radiation (IR) detector was used. Figure 18 is a photograph of the experimental set up used. Chao et al. [45] conducted orthogonal machining tests on the end of a tubular workpiece 228.6 mm (9 in) diameter and 20.64 mm (13/16) in wall thickness. Figure 19(a) and (b) show schematically the experimental

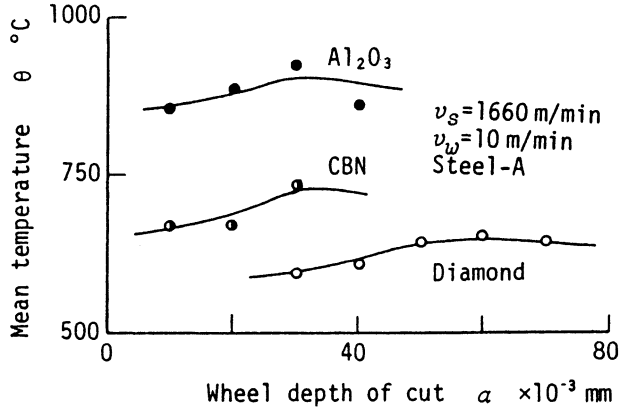

Fig. 26. Variation of mean temperature with the wheel depth of cut for different abrasives; after Ueda et al. [54].

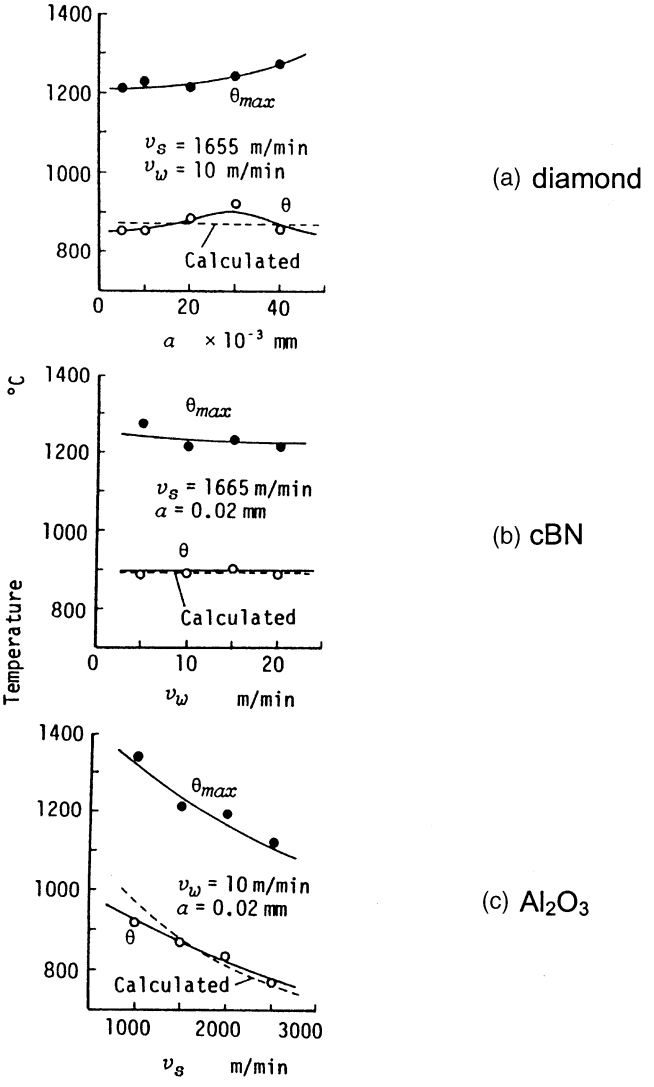

Fig. 27. Variation of the maximum temperature with wheel speed for (a) diamond, (b) cBN, and (c) Al_2O_3 abrasives; after Ueda et al. [54].

arrangement and the configuration of the sensor arrangement, respectively, after Chao et al. [45]. An axial slot of 38.1 mm (1.5 in) wide and 76.2 mm (3 in) long was provided in the wall to accommodate the photoconductive cell assembly. The radiant energy emitted at the tool flank was received by the sensor through 2.38 mm (3/32 in) diameter holes drilled axially in the tube wall. Alternately a hypodermic needle 0.127 mm (0.005 in) diameter and 19 mm (3/4 in) long could be used instead. The signal generated in the rotating sensor was brought out by a brush using a slip-ring assembly (copper rings and phosphor-bronze brushes).

As the workpiece was rotated, the flank face of the tool was scanned [effective view field fd in Fig. 19(b)], the output signal was displayed on an oscilloscope screen. For calibration, the cutting tool was resistance heated and the temperature measured using chromel–alumel thermocouples. Calibration of the end surface of the

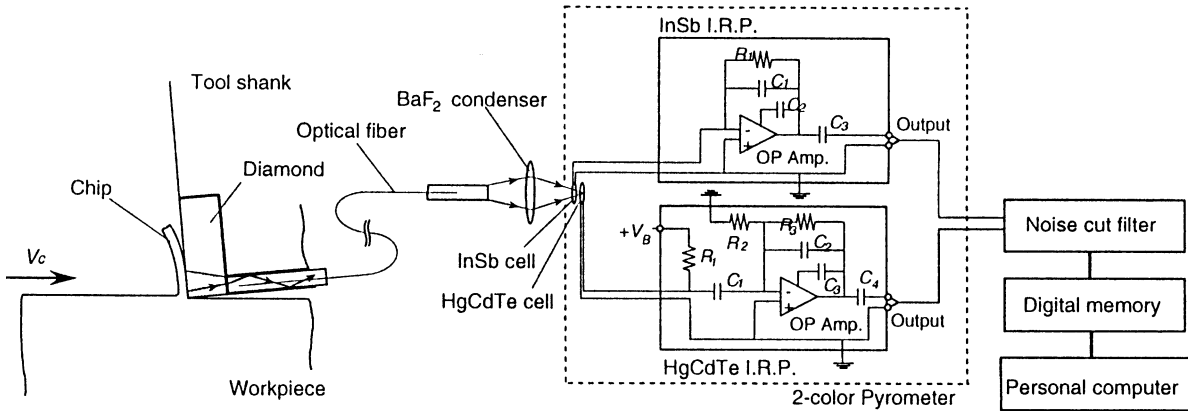

Fig. 28. Experimental set-up used in ultraprecision machining of aluminum to determine the temperature on the rake face; after Ueda et al. [56].

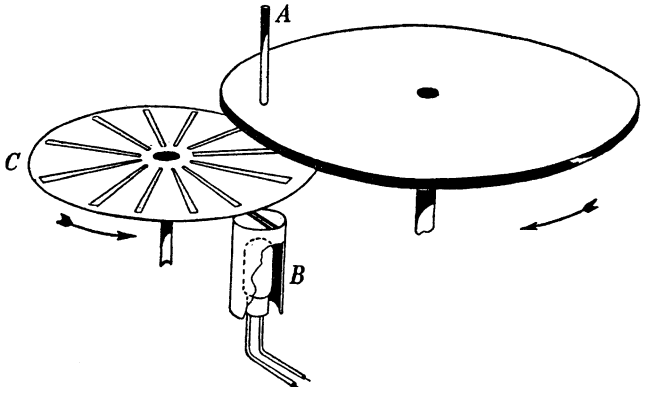

Fig. 29. Schematic of the experimental set-up used for the frictional hot spots using a PbS cell; after Bowden and Thomas [57].

carbide calibration strip was done directly on the lathe, duplicating the position of the tool flank. Figure 20(a) and (b) show the variation of the flank surface temperatures with the distance from the tool tip for different feeds [and a constant speed of 1.321 ms^{-1} (260 fpm)] when machining an AISI 1018 steel work material and at different speeds [and constant feed, 0.14 mm/rev (0.0055 ipr)] when machining an AISI 52100 steel work material, respectively. It can be seen from Fig. 20(a) and (b) that increasing feed or speed results in an increase of tool flank temperatures. There was also a gradual shift of the maximum temperature away from the tool edge.

Lenz [46] further modified the experimental setup of Kraemer [42] to determine the temperature distribution on the clearance face in longitudinal turning [Fig. 21(a)]. When turning a cylinder with a small slot, which is deeper than the depth of cut, the clearance surface becomes fully exposed and can radiate energy every time the slot crosses the clearance face. This enables a short emission of radiation to pass through the slot on the front surface of the cylinder where it is focussed and excites a photo diode. The time of exposure of the focused point on the clearance surface is very short (0.5–5 ms) when using a narrow slot. The diode can react rapidly during this very short time. Thus isotherms are established for the clearance surface of the tool as shown in Fig. 21(b). Lenz [47–49] also used the optical pyrometer technique to determine the temperature distribution at the chip–tool interface [Fig. 22(a)]. A PbS photoconductive infrared radiation detector was mounted in the cutting tool. The radiation was collected by an optical condenser through a hole in the tool reaching the rake face. The temperature field was determined by radial displacement of the tool (0.3 mm at a time) and by grinding off the 0.2 mm on the clearance face. Machining tests were conducted using steels (Ck45, XC45, and Ck60) using P10 and P30 cemented carbide tools. Figure 22(b) shows the temperature distribution on the tool face when machining XC 45 steel with a P30 cemented carbide tool. A scatter of ±3.5% is reported in spite of all the precautions. He considered this technique to be suitable only for laboratory studies in view of the extreme care required in assembling and using the set-up. Another disadvantage of this technique was the inability to measure temperatures closer than 0.45 mm to the cutting edge due to the design of the sensor.

Friedman and Lenz [50] used an IR optical pyrometer to determine the temperature field on the upper surface of the chip using a photo-sensitive PbS detector. Based on that work, they arrived at the following conclusions, some of which are somewhat opposite to the norm: (1) temperature increases almost linearly with the distance from the origin of the chip formation, (2) temperature increases with decrease in feed, (3) temperature decreases with increase in cutting speed, (4) variation of temperature with width is small except towards the edges, and (5) influence of tool material was negligible. Conclusions (2) and (3) are different from normal practice as the temperature generated should increase with increase in feed as well as speed. Conclusion (2) may be due to increased rubbing with decrease in feed. Both conclusions may have something to do with the IR optical pyrometer technique used as it is difficult to explain the results reported.

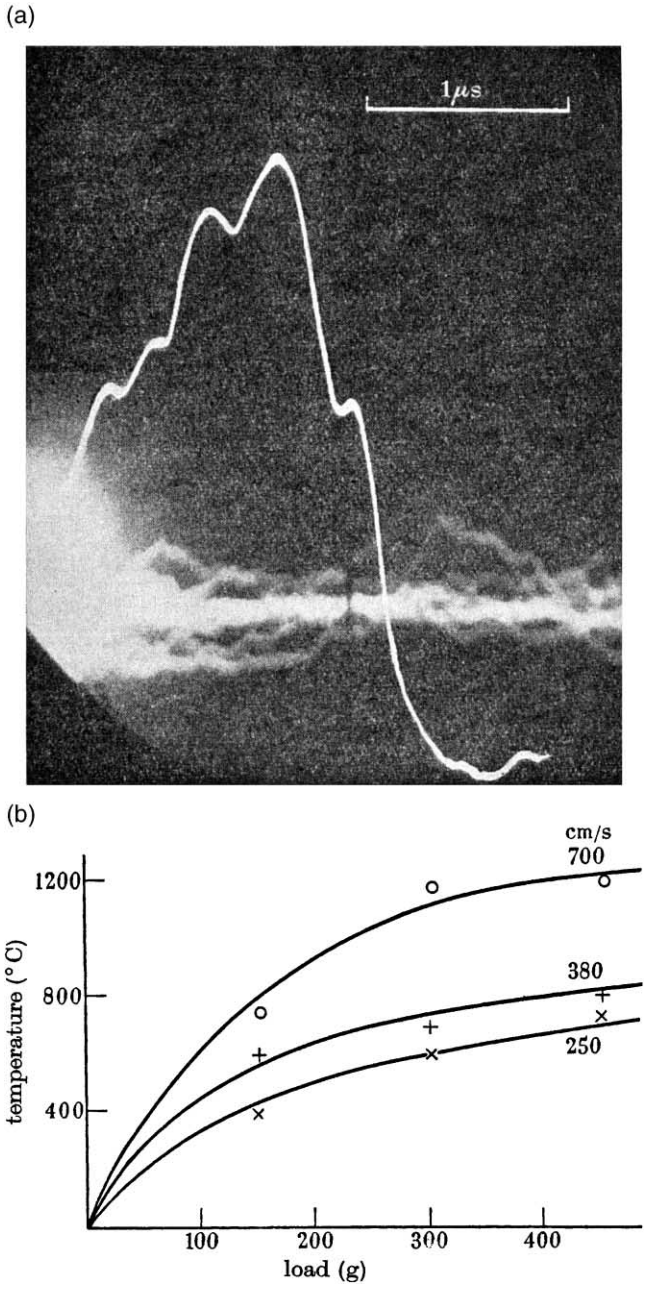

Fig. 30. (a) Cathode-ray oscilloscope trace of radiant energy from a single hot spot developed between a steel slider and a rotating glass disk under a load of 3.43 N (350 g) and a sliding speed of 0.7 ms^{-1}; (b) variation of the maximum temperature of hot spots with load and sliding speed for steel sliding on glass; after Bowden and Thomas [57].

Prins [51] considered the influence of wear on the temperature distribution at the rake face of the tool in cutting using an infrared pyrometer focused at the rake face through holes in the chip. These holes were drilled parallel to the axis of rotation, so that chips, with holes at a certain distance from each other, are produced. The temperature in the whole contact area is measured by changing the positions of the holes along the width of the chip, and moving the pyrometer perpendicular to the cutting edge. The influence of tool wear, tool geometry, feed, and cutting speed on the temperature distribution were investigated. Some of his conclusions resulting from this study are the following: (1) the maximum tool temperature to increase with speed and feed, as can be expected, (2) maximum temperature at the tip of the tool is lower than in the middle of the depth of cut along the rake face, (3) a larger corner radius can reduce the temperature of the tool tip, and (4) a larger included angle and a smaller cutting edge angle reduces the temperature of the tool tip.

Ueda et al. [52] measured the temperature of the abrasive grains on the wheel surface using an InAs infrared detector. Figure 23(a) and (b) show a schematic of the radiation pyrometer system used and the experimental grinding setup, after Ueda et al. [52]. The infrared energy radiated from the abrasive grains passes through the target area of the optical fiber (which can accept only rays radiated from the target area) and is transmitted via the optical fibers to the InAs detector. The infrared energy is converted to electrical signal, amplified, and displayed on a computer. An optical fiber accepts the infrared flux radiated from the abrasive grains and transmits it to the detector. The pyrometer makes it possible to observe the history of each cutting grain on the wheel surface. They used an AISI 1055 steel (hardness: 200 VHN) work material and an aluminum oxide grinding wheel (A36K7VC). The wheel speed and the work speed were 28.85 ms^{-1} and 0.167 ms^{-1}, respectively. The wheel down feed was 20 μm. They found the temperature of the abrasive grains at 4.2 ms after grinding to be distributed in the range of 500°C to 1400°C, with a mean temperature of 820°C. In a subsequent investigation, Ueda et al. [53] compared their temperature measurements with the IR pyrometer with those of a thermocouple. They found the thermocouple formed by spot welding to be inferior in response speed and less accurate in registering heat pulses.

Ueda et al. [54] used an infrared radiation pyrometer to determine the grinding temperature on the surface of a ceramic workpiece ground by a diamond grinding wheel. The work materials used were Si_3N_4, SiC, and Al_2O_3. They devised a new type of infrared (IR) pyrometer in which an optical fiber accepts the infrared flux radiated from the object and transmits it to an infrared (IR) detector InSb cell. The time constant of the InSb cell is ~1 μs and the flat response of the amplifier of the IRP is lower than 100 kHz. The pyrometer is connected by two types of optical fiber — a fluoride fiber and a chalcogenide fiber. With these fibers, it was possible to measure lower temperatures than with quartz fibers, since these fibers can transmit infrared rays of longer wavelengths. This pyrometer is suitable for measuring temperature of a very small object whose temperature changes rapidly. Figure 24(a) and (b) are schematics of the pyrometer system and the experimental set-up used,

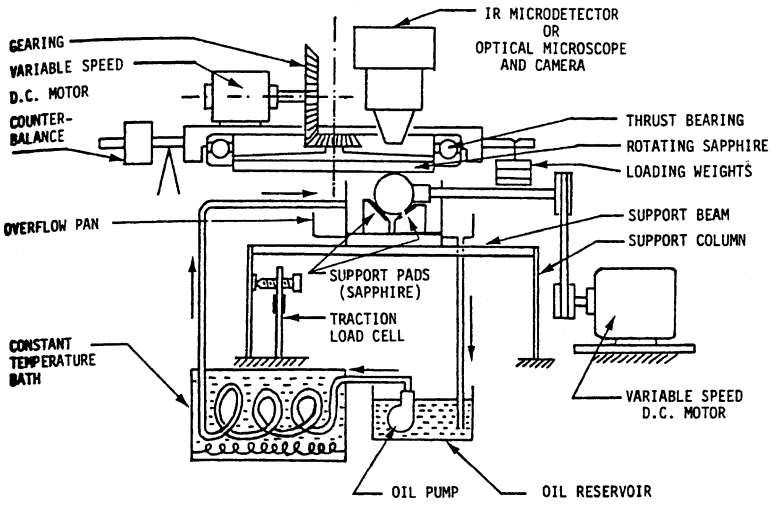

Fig. 31. Schematic of the combined rolling and sliding EHD contact simulation apparatus used to directly measure the surface temperature in elastohydrodynamic (EHD) contacts by an infrared (IR) radiation microdetector; after Nagaraj et al. [59].

respectively, after Ueda et al. [54]. Figure 25(a)–(c) show the variation of the temperature with the depth below the ground surface for Si_3N_4, SiC, and Al_2O_3, respectively. Highest temperature was obtained with Si_3N_4 work material whose grinding power was largest. This was estimated to be 800°C by extrapolation of the data in Fig. 25(a).

Ueda et al. [55] experimentally determined the temperature of the abrasive grains in a grinding wheel using an infrared radiation pyrometer with optical fibers and an InAs cell. Three types of grinding wheels, namely, Al_2O_3, cBN, and diamond were used in grinding an AISI 1055 steel work material of two hardness values, namely, 200 and 570 VHN. Figure 26 shows the variation of mean temperature with the wheel depth of cut for different abrasives. It can be seen that the mean temperature is highest with Al_2O_3, followed by cBN, and diamond. This seems to follow the increase in the thermal conductivity as one goes from Al_2O_3 to cBN, to diamond. Also, the mean temperatures do not seem to depend much on the wheel depth of cut. Figure 27(a)–(c) show the variation of the maximum temperature with wheel speed for Al_2O_3, cBN, and diamond abrasives. The maximum temperature of the abrasive grains at the cutting point was found to reach close to the melting temperature of the work material.

Ueda et al. [56] used an optical pyrometer to determine the temperature on the rake face of a single crystal diamond tool in ultraprecision machining of aluminum. The infrared rays radiated from the chip–tool contact area, and transmitted through the diamond tool, are collected by a chalcogenide fiber and led to a two-color detector which consists of InSb and HgCdTe detectors. The two-color pyrometer can measure the temperature regardless of the size of the object, when the temperature of the object is constant. When the object has a surface of known temperature distribution, it is possible to estimate the maximum temperature from the measured temperature. Figure 28 shows the experimental set-up used in ultraprecision machining of aluminum to determine the temperature on the rake face, after Ueda et al. [56]. Aluminum was precision turned dry (or without a cutting fluid), using a single crystal diamond tool ($-5°$ rake and $5°$ clearance) at a depth of cut of 10 μm and cutting speed of 6.67–15 ms^{-1}. The temperature on the rake face of a diamond tool was shown to increase with increase in the cutting speed and reaches a maximum value of ~190°C.

In the field of tribology, Bowden and Thomas [57] investigated the surface temperature developed at the rubbing contact between a metal and a transparent solid (e.g. glass) by measuring the infra-red radiation transmitted through the solid. They used a PbS cell with a time constant of 10^{-4}s at 20°C and a peak sensitivity in the neighborhood of 2.7 μm. Figure 29 is a schematic of the experimental set-up used for the frictional hot spots using a PbS cell after Bowden and Thomas [57]. The lower sliding surface is a glass disk that is rotated by a motor to give linear speeds ranging from 0.1 to 0.7 ms^{-1}. The upper surface which is usually of a metal is a cylinder A, with the flat end (≈1 mm diameter) sliding on the glass. It is held in a pivoted arm and weights up to 4 kg can be placed directly on it. The photosensitive cell B is enclosed in a brass holder below the disc. On top of this holder is a narrow slit in line with the direction of motion. The output of the transducer is amplified and observed on a cathode-ray oscilloscope (CRO). Between the glass disk and the PbS cell, a chopper C is placed so that the radiation may be chopped at about 3 kHz.

Figure 30(a) is a cathode-ray oscilloscope (CRO) trace of radiant energy from a single hot spot developed

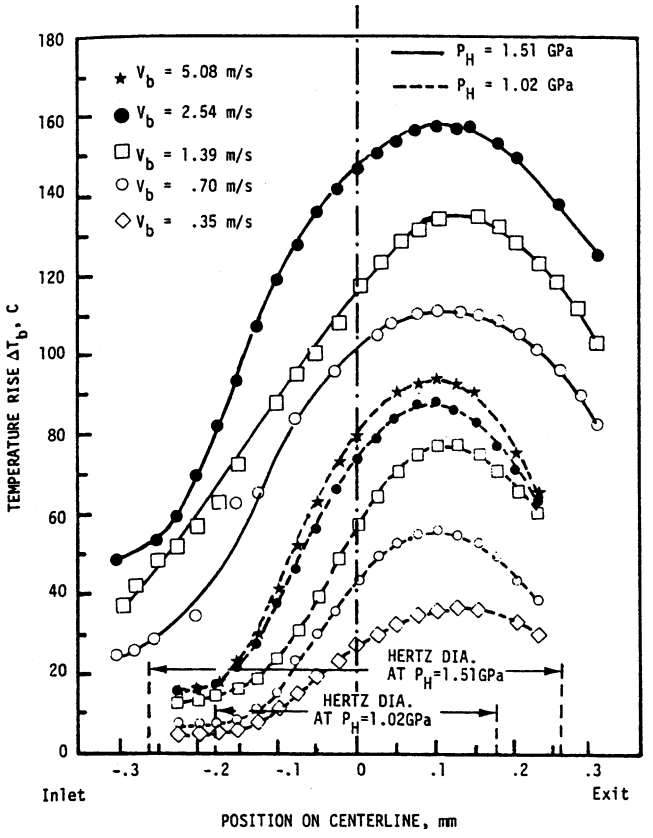

Fig. 32. Variation of ball surface temperature rise along the contact center-line as a function of contact position, Hertzian contact pressure, and velocity for the case of pure sliding (sapphire surface stationary); after Nagaraj et al. [59].

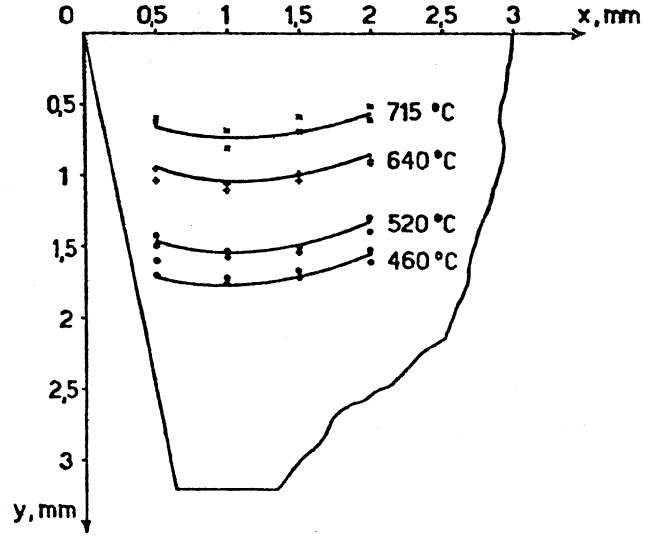

Fig. 33. Experimental data and corresponding isotherms; after Rossetto and Koch [64]. Workmaterial: AISI 1040 steel; tool: cemented carbide (P20); depth of cut: 2 mm; feed: 0.428 mm/rev; cutting speed: 3.33 ms^{-1}.

Table 2
Powders of chemicals used and respective melting points

Chemical symbol	Melting point °C	Boiling point °C
NaCl	800	1413
KCl	776	1500
CdCl	568	960
$PbCl_2$	501	954
AgCl	455	1550
Zn	419	907
KNO_3	339	–
Pb	327.4	1750
$SnCl_2$	246.8	623
Sn	231.9	2270

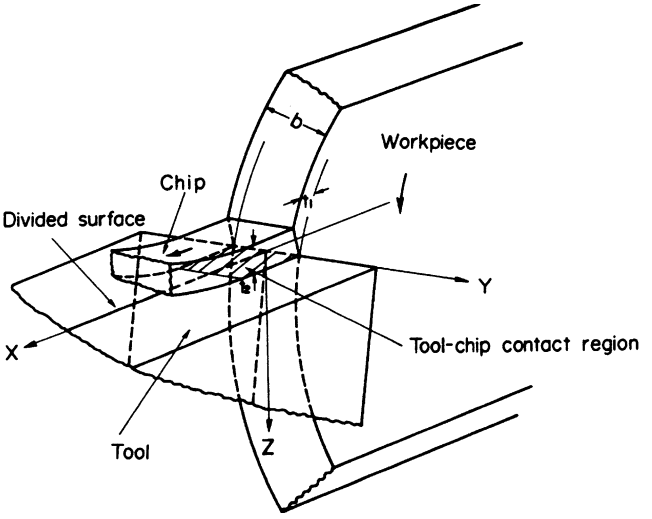

Fig. 34. Schematic of the experimental method used for determining the temperature distribution in the tool using a sandwich tool containing fine powder of a compound of constant melting point; after Kato et al. [65].

between a steel slider and a rotating glass disk under a load of 3.43 N (350 g) and a sliding speed of 0.7 ms^{-1}. The time of sweep of the oscillograph was 5 ms. The system was calibrated using a heated platinum wire 1.8 mm (0.071 in) in diameter behind a hole of 1.42 mm (0.056 in) in diameter as an artificial hot spot. Figure 30(b) shows the variation of the maximum temperature of hot spots with load and sliding speed for steel sliding on glass. The form of these curves was found to be somewhat influenced by the softening temperature of glass (≈800°C) but the dependence of the temperature on load, speed, and thermal properties of the rubbing solids was consistent with the theory. The local surface temperatures were high and fluctuating, and the maximum temperature rise was in general limited by the melting point of the metal. They also found occasional hot spots of very high temperatures with metals that readily oxidize. This was attributed to the exothermic reaction of the metal with the oxygen of the air and consequent increase in the thermal energy.

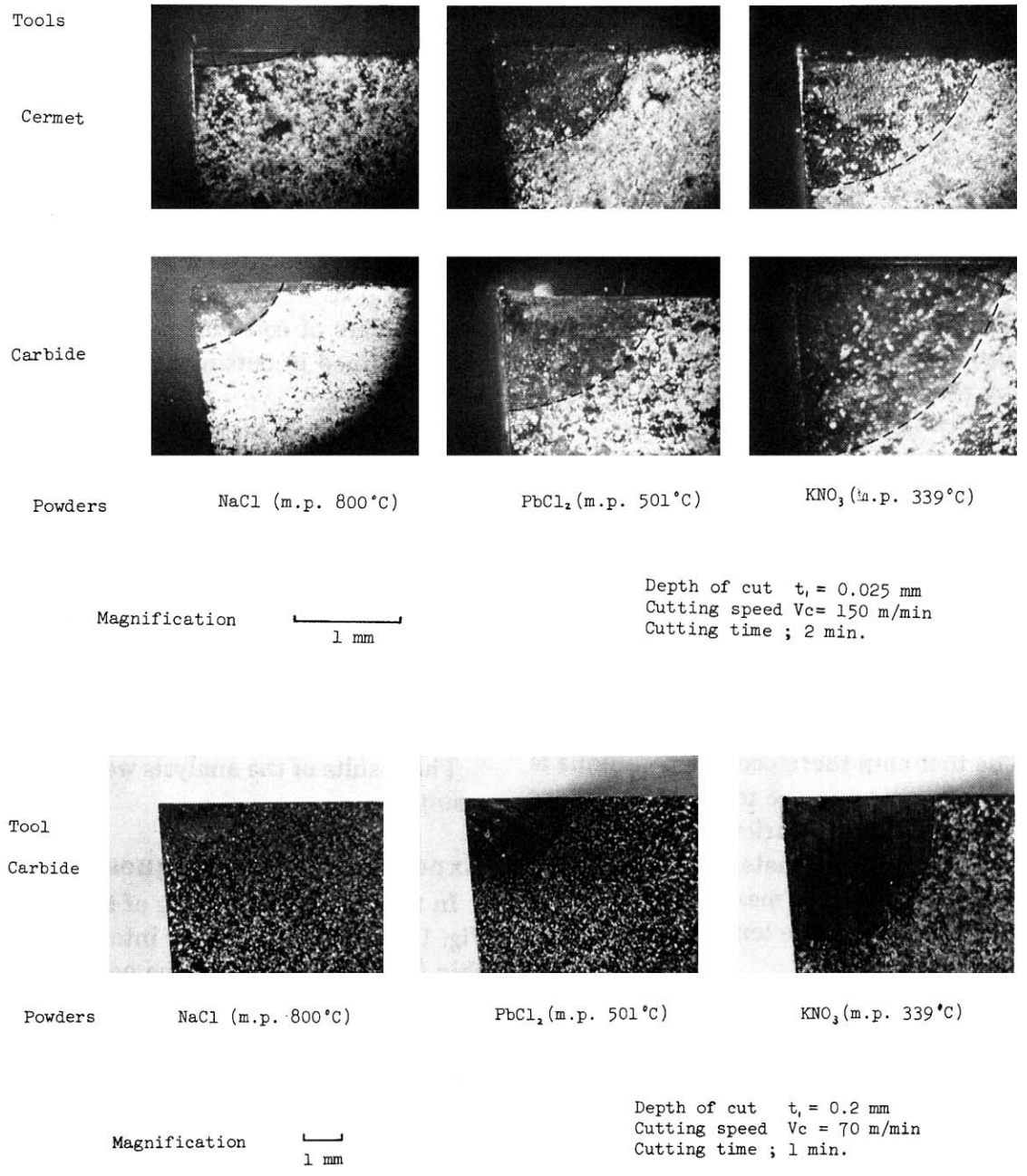

Fig. 35. Optical micrographs of the sandwich surface of the tool for two different cutting speeds (lower) 1.16 ms^{-1}, and (upper) 2.5 ms^{-1}, using powders of three chemicals (NaCl, $PbCl_2$, and KNO_3) of melting points 800°C, 501°C, and 339°C, respectively; after Kato et al. [65].

Parker and Marshall [58] investigated experimentally the temperatures generated at sliding surfaces, especially between railroad wheels and the brake blocks, using an optical pyrometer which covered a range from 200–900°C with a response time of 10^{-3} s. The pyrometer was used to measure the temperatures of the wheel and the brake during brake applications, just as it emerged beneath the brake block under various conditions. Surface temperatures of the raised areas of the wheel were reported to increase with the kinetic energy dissipation, and for conditions which may be regarded as moderate in service, temperatures of 800°C were recorded. Such high temperatures were shown to be responsible for the inconsistency in the kinetic coefficient of friction, for the initiation of rapid wear of the block, and the production of hot-spots on the wheel which ultimately may lead to cracks. Also, the nature of distortion of the wheel may react unfavorably on the rails. They also investigated the variation and extent of the contact between the brake block and the wheel. They concluded that high wheel surface temperatures (800°C) are a result of "strip braking". By reducing the length of the strip to half, or, even a quarter of the original length, they were able to eliminate the deleterious formation of martensite, such as hot

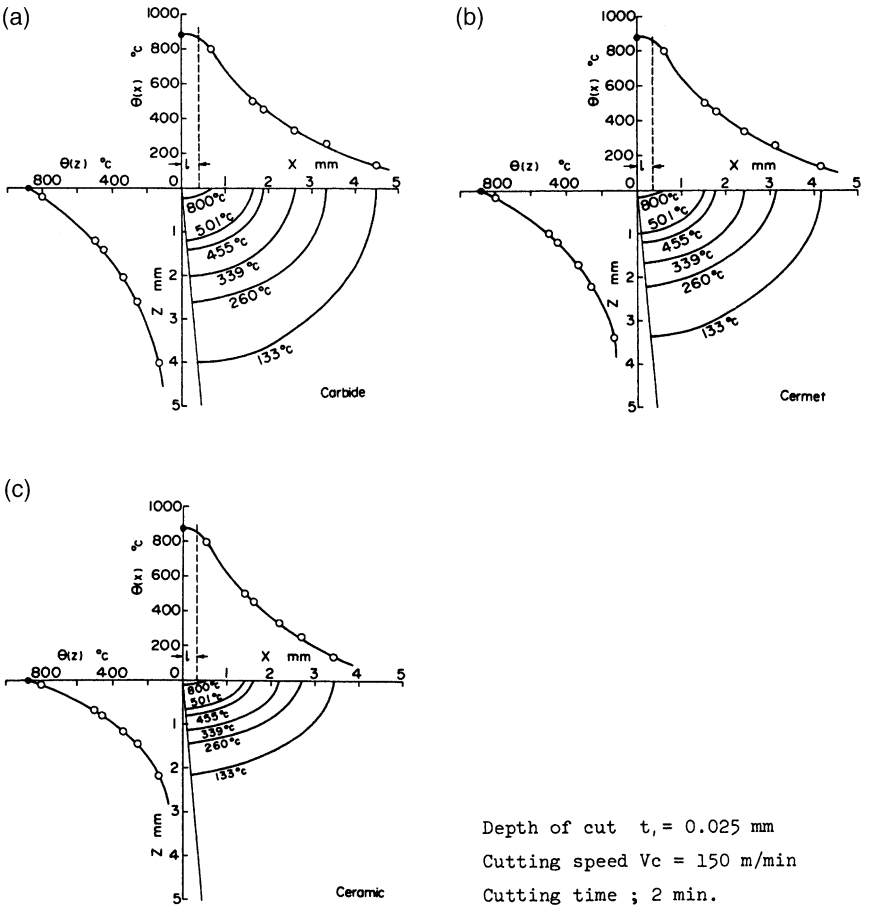

Fig. 36. Temperature distributions along the rake face (*x*-direction) and the clearance face (*z*-direction) for (a) carbide, (b) cermet, and (c) ceramic tools, respectively; after Kato et al. [65].

Table 3
Melting point and purity of PVD film materials

PVD film material	Symbol	Melting point K	Purity %
Germanium	Ge	1211	99.999
Antimony	Sb	904	99.9999
Tellurium	Te	723	99.999
Lead	Pb	601	99.999
Bismuth	Bi	545	99.999
Indium	In	429	99.999

spots and finally cracks, thus reducing wear significantly. Furthermore, since the cost of the brake is somewhat proportional to its size, reducing the length can be more economical.

Nagaraj et al. [59] used an infrared (IR) radiation microdetector to directly measure the surface temperature in elastohydrodynamic (EHD) contacts. Figure 31 shows a schematic diagram of the combined rolling and sliding EHD contact simulation. The EHD contact was formed using a ball (31.8 mm in diameter) loaded against a sapphire disk (89 mm in diameter×3 mm thick) with a surface roughness of 6 nm Ra. Chrome steel balls (AISI 52100) of three different roughness values, namely, 0.011, 0.075, and 0.38 μm Ra (referred to as smooth, medium, and rough, respectively) were used. The infrared radiation emitted at the contact was measured with an infrared radiometric detector having a spot size resolution of 38 μm. The contact temperatures deduced from these readings are time-averaged values since a large number of surface asperities will pass through the field of view during the sampling interval. The fluid used was a naphthenic base oil with a peak emission spectra at 3.4 μm. The wide band optical (3.7–5.2 μm) filter was used to eliminate the oil emission peak. Fig. 32 shows the variation of ball surface temperature rise along the contact center-line as a function of contact position, Hertzian contact pressure, and velocity for the case of pure sliding (sapphire surface stationary) after Nagaraj et al. [59]. The base shapes of the curves are all similar, showing a maximum (up to 300°C) just downstream of the contact center. According to the authors, the analysis of their experimental data showed good correlation with Blok's flash temperature theory for simple sliding.

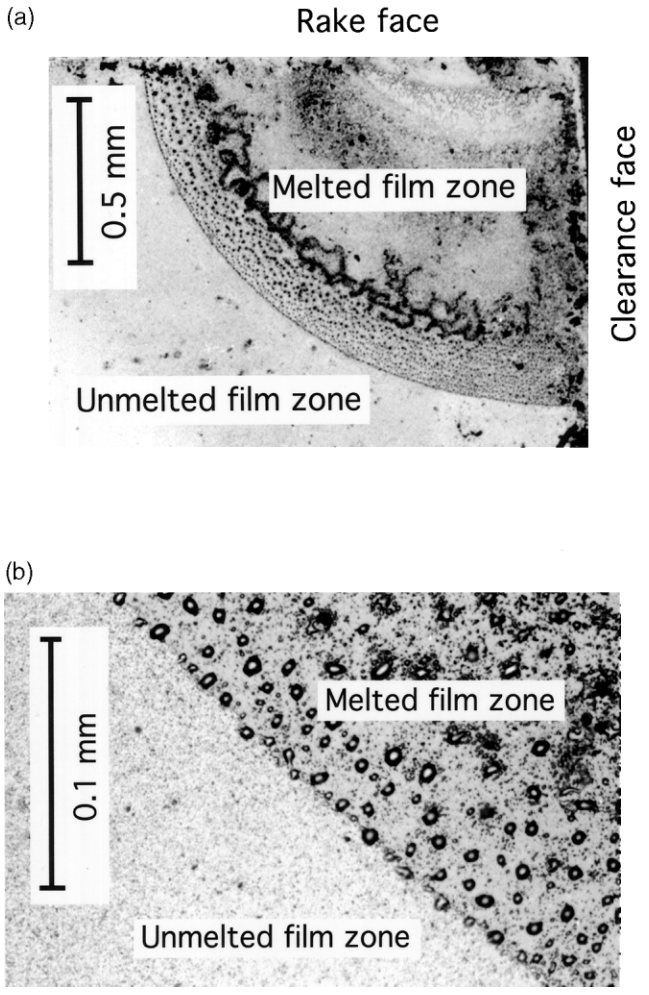

Fig. 37. Photomicrographs at two magnifications, (a) and (b), of the PVD coated (tellurium) sandwich surface on a carbide tool after cutting at 3.33 ms^{-1} with a feed rate of 0.2 mm/rev and a width of cut of 2 mm for a cutting time of 5 s; after Kato et al. [65].

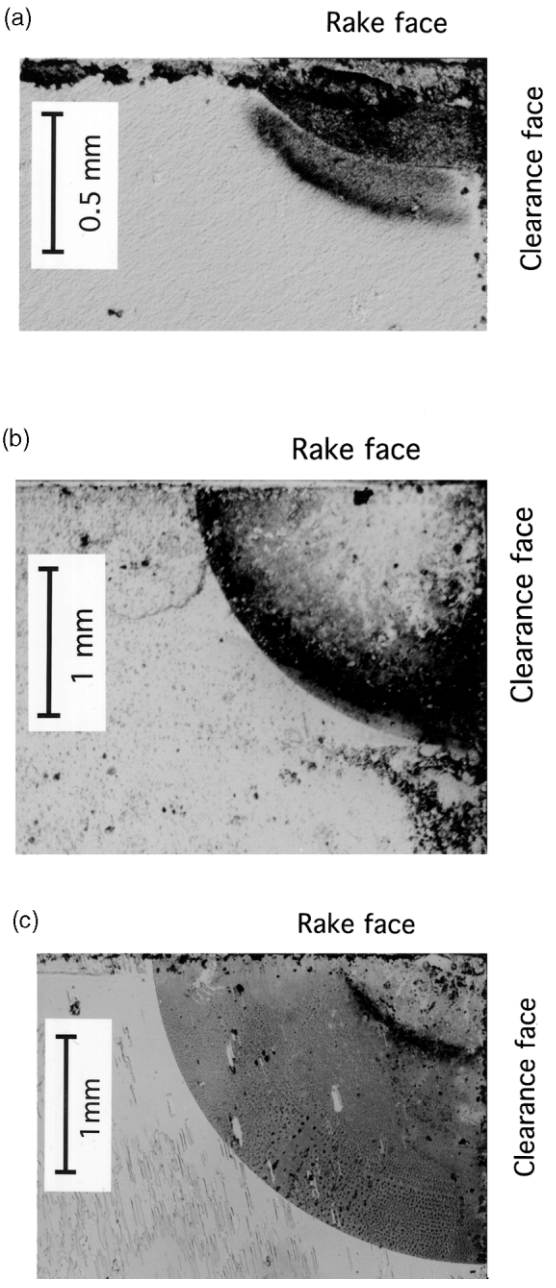

Fig. 38. Optical micrographs of the PVD coatings of (a) germanium, (b) lead and (c) bismuth; after Kato and Fujii [66].

Suzuki and Kennedy [60] developed an ingenious method to detect flash temperatures in a sliding contact by tribo-induced thermoluminescence, i.e., light emitted when a material is stressed to the point of fracture. The actual application involved a spherical sapphire slider moving rapidly on a thin film magnetic disc. Even though flash temperatures at hot spots may emit high-temperature visible light, the hot spots are generally so small and are in contact for such a short duration that they do not give off enough energy to be seen with a naked eye. Instead, a photomultiplier is used to collect the photons emitted by a hot spot. A photomultiplier offers many advantages over an IR detector for this application, including a response time of 100 ns; output can be amplified by a factor of 10^5; and a single photon can be detected. Flash temperatures of 1000°C and lasting 2 μs at the sliding interface were reported.

3.4. Thermal paints

Use of thermal sensitive paints is one of the simplest and most inexpensive techniques to estimate the temperature of a cutting tool during machining. It depends on the ability of a given paint to change its color due to chemical action at a given temperature. Different thermal sensitive paints respond to different temperatures. Much depends on the heating rate as well as the duration. Therefore, the application of this technique is generally limited to controlled heating conditions. Most researchers use this technique to estimate the tempera-

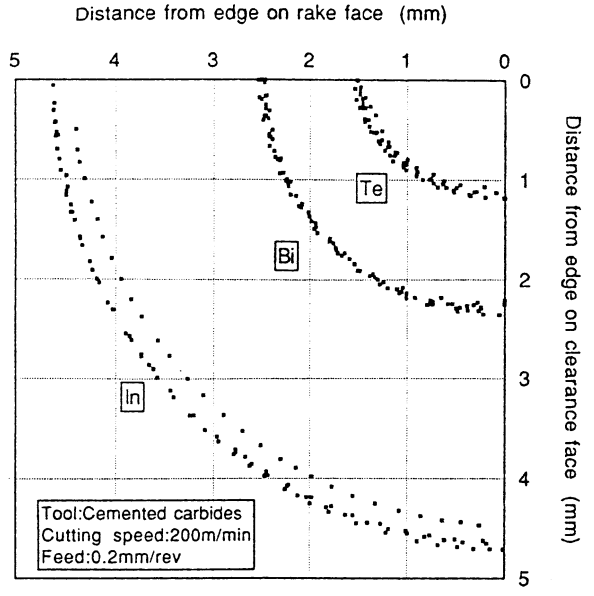

Fig. 39. Temperature contours in the tool after the cutting tests; after Kato and Fujii [66].

tures in accessible surfaces of the tool or the workpiece. This technique was used successfully by some researchers including Schallbroach and Lang [61], Bickel and Widmer [62] and others. The results obtained with this technique are generally considered preliminary and some other technique is used for confirmation. Okushima and Shimoda [63] used this technique to determine the temperature distribution within a tool using a split-tool with the paint applied at the joint. Rossetto and Koch [64] investigated the temperature distribution on the tool flank surface using thermal sensitive paints. The functional relationship between the temperature on the tool flank surface and the cutting variables was obtained using the multiple regression method. Figure 33 shows the experimental data and corresponding isotherms, after Rossetto and Koch [64]. This was followed by the work of Kato et al. [65] who used powers of different melting points, which will be covered in the following.

3.5. Temperature distribution using fine powders of constant melting point

Kato et al. [65] developed an experimental method for determining the temperature distribution in the tool using a sandwich tool containing fine power of a compound of constant melting point. The method involves identification of the boundary between the melted and unmelted powder. Table 2 gives a list of various compounds (along with their melting and boiling points) used in this investigation. A compound with different melting point is used in each test. The temperature isotherms are drawn by superimposing the boundary lines obtained in various tests. Since these materials have constant melting points, there is no need for any calibration. The average size of

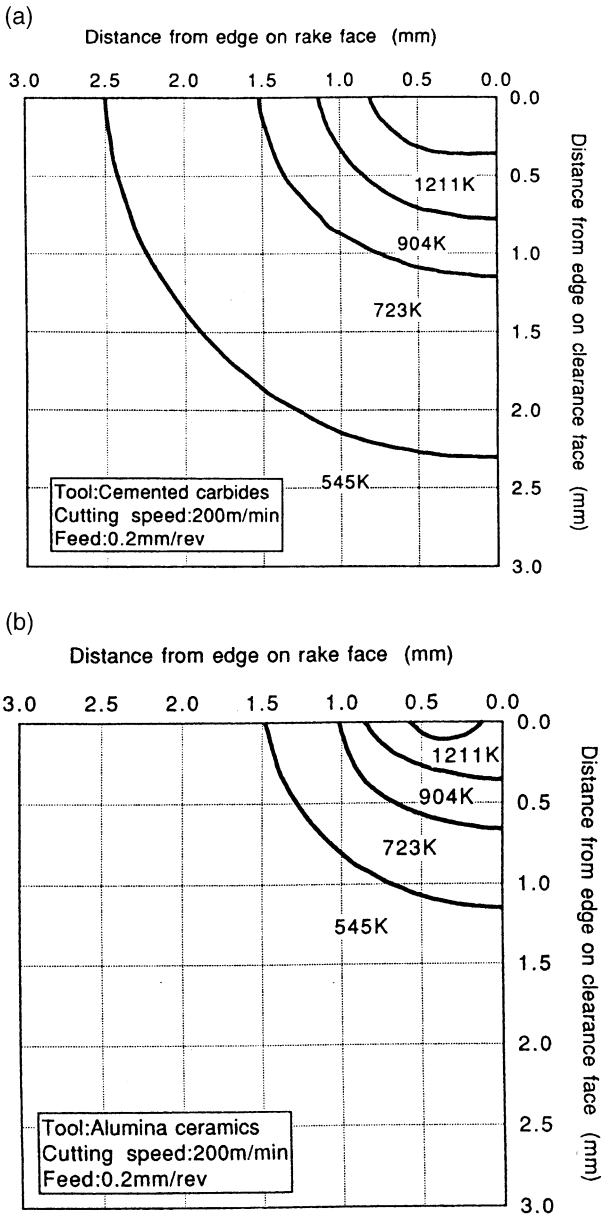

Fig. 40. Temperature contours obtained using two different tool materials, (a) cemented carbide and (b) alumina ceramic; after Kato and Fujii [66].

the powders used was 10–20 μm. The powders were applied to the sandwich tool in an aqueous solution of sodium silicate to ensue adhesion of the powder to the tool. The two halves of the tool were then put together prior to cutting. Orthogonal cutting experiments were performed on one end of a tube of an AISI 1025 steel 2 or 4 mm thick (see Fig. 34 for details). The tool materials used were carbide (P20), cermets, and ceramics with a rake angle of 0° and a clearance angle of 5°.

Figure 35(a) and (b) show optical micrographs of the sandwich surface of the tool for two different cutting speeds (1.167 ms^{-1} and 2.5 ms^{-1}.) using three powders (NaCl, $PbCl_2$, and KNO_3) of melting points 800°C,

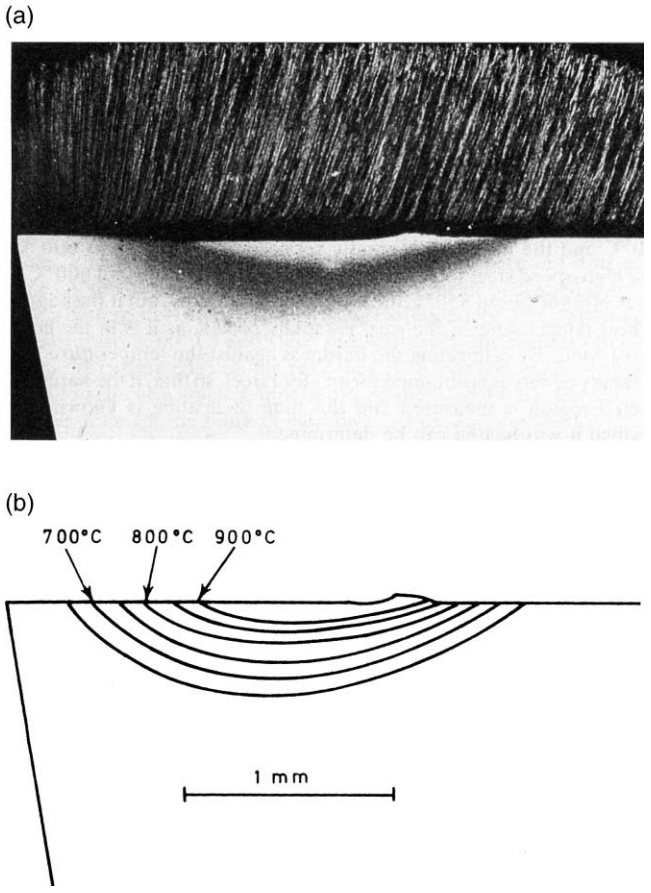

Fig. 41. Photomicrograph of a polished and etched (in nital) cross-section of a high-speed steel tool used in the machining of iron at 3.048 ms^{-1} (600 fpm) at a feed rate of 0.25 mm/rev (0.010 ipr), and depth of cut of 1.25 mm (0.05 in) for a cutting time of 30 s; after Trent and Wright [68].

501°C, and 339°C, respectively, after Kato et al. [65]. The white regions on the photographs are the unmelted regions. It can be seen that the tool surface clearly consists of two zones, namely, the melted zone and the unmelted zone with the boundary distinctly discernible as shown by the dotted lines in the photographs. The temperature contours can be obtained by superimposing the isothermal lines obtained with powders of different melting points in each test. Figure 36(a) and (c) show the temperature distributions along the rake face (*x*-direction) and the clearance face (*z*-direction) for carbide, cermet, and ceramic tools, all at the same cutting conditions as given in the figure. It can be seen that the temperature distribution within the tool differs for each tool material. For example, the gradient is much steeper with the ceramic tool than with the cermet or the carbide tool. This is due to poor thermal conductivity of the ceramics compared to the other two materials. At the same time, as can be expected, there is not much difference in the maximum temperature on the rake face in the vicinity of the cutting edge amongst the three tools with the maximum temperature of ~900°C.

3.6. Temperature distribution using PVD coatings of materials with known melting temperatures

Kato and Fujii [66] improved on the technique developed by Kato et al. [65] using a physical vapor deposition (PVD) coating instead of applying fine powders to the sandwich tool in an aqueous solution, as the thermal sensor. The thermal response with the PVD coating was considered superior to that of the powders, as the powders formed a thick porous layer and may not have established a close contact with the tool sandwich surfaces. Table 3 gives various PVD coating metals used along with their respective melting temperatures and purity. Orthogonal cutting experiments were conducted by feeding the split sandwich tool radially inwards on a disc. Figure 37(a) and (b) show photomicrographs at two magnifications of the PVD coated (tellurium) sandwich surface on a carbide tool after cutting at 3.33 ms^{-1} with a feed rate of 0.2 mm/rev. and a width of cut of 2 mm for a cutting time of 5 s. It can be seen that the boundary between the melted and unmelted region is again clearly discernible. The boundary is the isotherm of 723 K, the melting temperature of tellurium. The temperature contours are established using PVD films of different metals as given in Table 3. Figure 38(a) to (c) are the optical micrographs of the PVD coatings of germanium, lead and bismuth, respectively, and Fig. 39 shows the temperature contours after the cutting tests. Figure 40(a) and (b) show the temperature contours obtained using two different tool materials, namely, cemented carbide and alumina ceramic, respectively. It can again be seen that the temperature gradients are much steeper with the ceramic tool due to poor thermal properties compared to the cemented tungsten carbide tool.

3.7. Temperature distribution using metallographic methods

Wright and Trent [67] developed a metallographic technique for determining the temperature gradients in high speed steel (HSS) cutting tools. The temperature near the rake face is determined either by observing the known microstructural changes in the high-speed steel tool (HSS) after cutting, or by measurement of changes in hardness using a microhardness test. They estimated that they can determine temperature in the range of 650–900°C with an accuracy of ±25°C. Figure 41 is a photomicrograph of a polished and etched (in nital) cross-section of a high-speed steel tool used in the machining of iron at 3.048 ms^{-1} (600 fpm) at a feed rate of 0.25 mm/rev (0.010 ipr), depth of cut 1.25 mm (0.05 in) for a cutting time of 30 s [68]. Note that this speed is far higher than the normal speeds used in the cutting of steel with a HSS tool. Higher magnification of this reveals structural changes in the HSS which can be related to the temperature generated. By calibrating the microstruc-

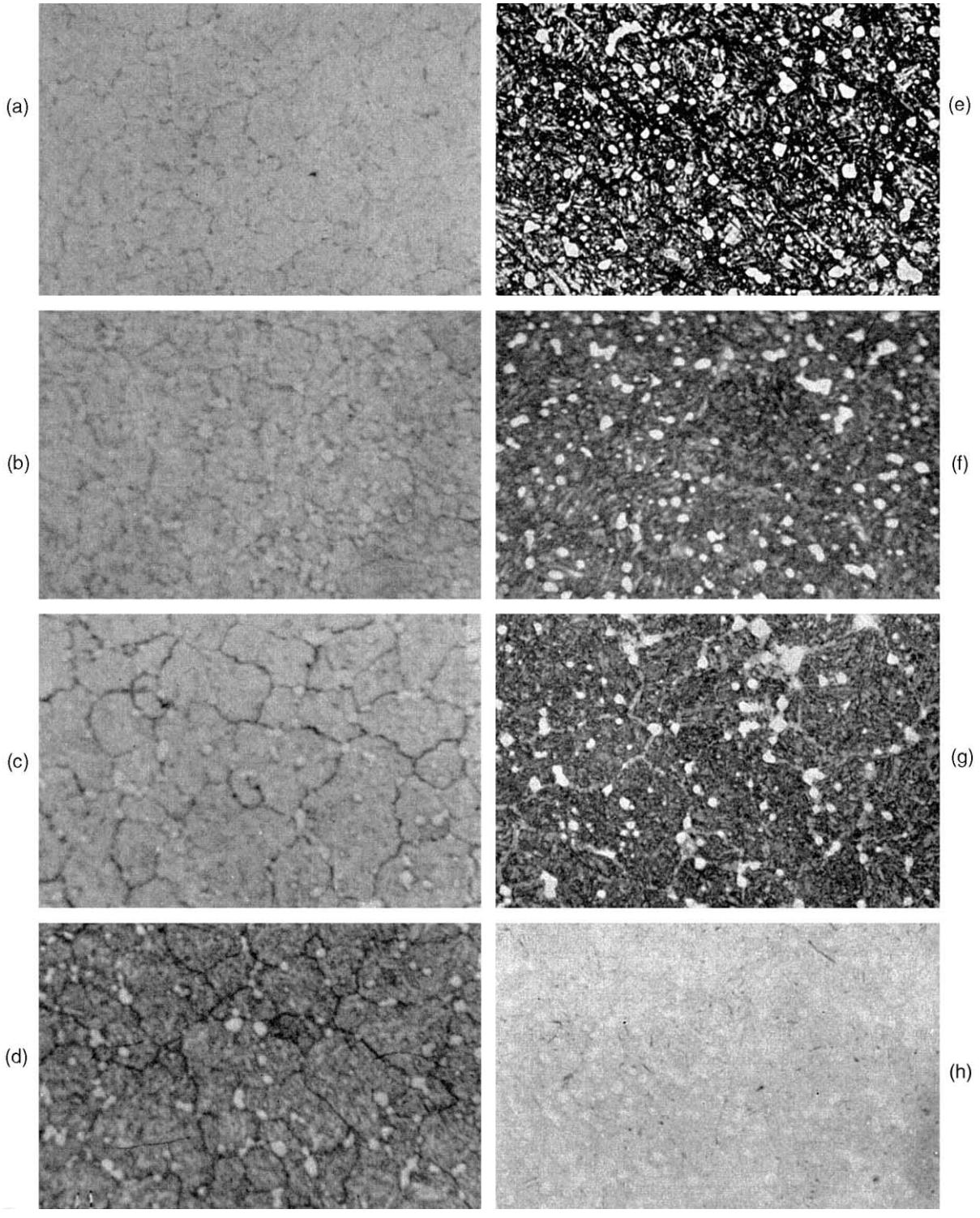

Fig. 42. Calibration of the microstructure of the HSS after heating at different temperatures from 600–900°C; after Wright and Trent [67].

ture of the HSS after heating at different temperatures from 600–900°C (Fig. 42) and comparing it with the microstructure obtained after cutting, the temperature distribution can be determined. Figure 43 shows the temperature isotherms in the tool deduced from the structural changes.

While the technique developed by Wright and Trent [67] for the determination of temperature distribution is ingenious, it is applicable only to those materials that exhibit a change in microstructure with temperature, such as HSS tools. Consequently, other tool materials, such as cemented carbide, or ceramics, cannot be used

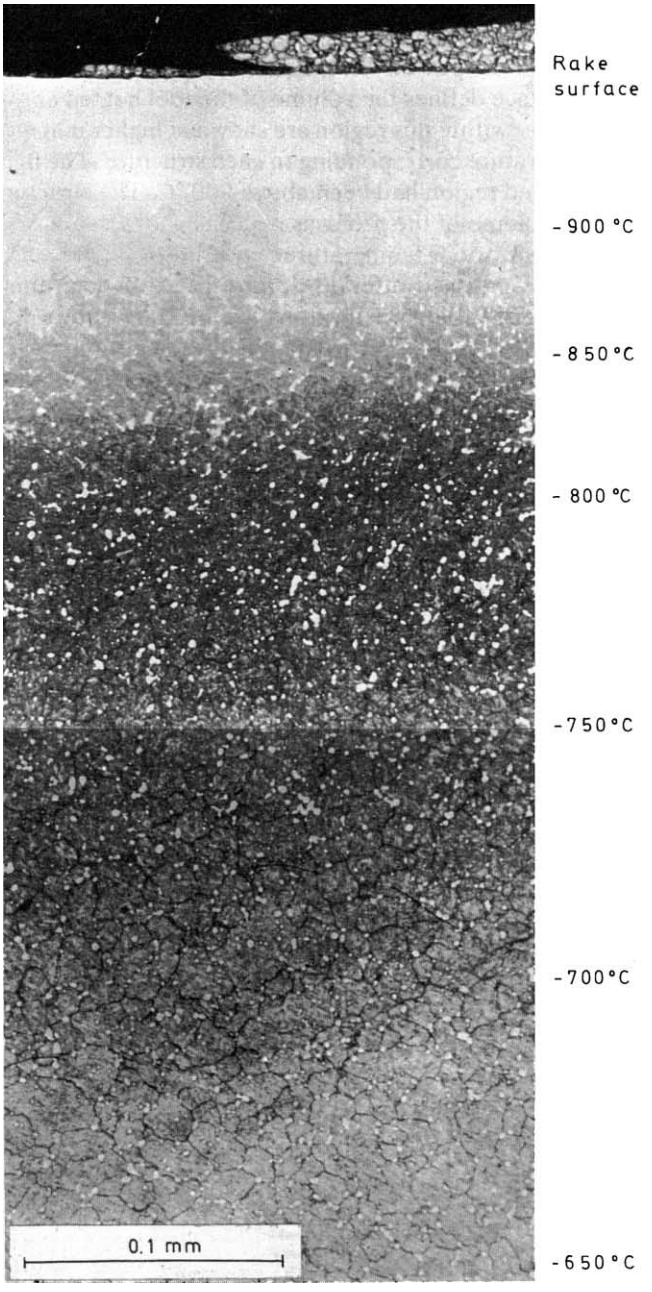

Fig. 43. Temperature isotherms in the tool deduced from the structural changes; after Wright and Trent [67].

for this method. Also, the cutting tests have to be carried out at high cutting speeds under which the HSS tools can wear rapidly. Further, as the changes in the microstructure depend not only on the temperature (and sufficient time for the transformation to take place completely) but also on the rate of cooling period, several calibrations have to be performed to obtain good correlation. Nevertheless, this is an important contribution towards an attempt to determine the temperature distribution in cutting.

4. Concluding remarks

It can be seen from the above review of the literature on the various methods of temperature measurements, an appropriate technique for a given thermal problem depends on the situation under consideration, such as the ease of accessibility of the sensor to the location of the subject, spot size, dynamics of the situation, accuracy needed, cost of instrumentation, advancements in sensor technology, and data collection and analysis. Some techniques can be quite simple (e.g. thermal paints) but may not be very accurate and can be subject to errors. Some techniques (e.g. temperature distribution using metallographic techniques) can be used only for specific materials where change in temperature leads to change in the microstructure (HSS). Even for this case, the cutting conditions have to be much higher than normal to obtain such a transformation in the microstructure. Optical and infrared radiation pyrometers require elaborate instrumentation and may require a special environment in some cases. Advancements in the sensor technology, signal transmission via optical fibers, and detection systems are enabling increasing use of this technique for a range of manufacturing operations, such as grinding of metals, glasses, and ceramics with various types of grinding wheels (Al_2O_3, cBN, and diamond). While some techniques give average values under quasi steady conditions (e.g. chip–tool thermocouples) others can provide dynamic values or flash temperatures with a fast response time (e.g. Suzuki and Kennedy's [60] tribo-induced thermoluminescence). Some techniques require quite elaborate preparation (e.g. temperature measurement using fine powders of constant melting point, or embedded thermocouples with various holes drilled in the cutting tool) while other techniques require expensive instrumentation (optical and infrared pyrometers). Advancements in the sensor technology (e.g. thin film technology) are enabling the use of rather inexpensive sensors at appropriate locations (e.g. temperature measurement using PVD coatings of materials of known melting temperatures). Also, incorporation of microelectronic circuits close to the cutting edge is enabling sensor data to be gathered without the need for elaborate instrumentation. This also increases the sensor signal to noise ratio, thus increasing the accuracy of measurement. Some techniques can only provide a temperature at a given location or a given region (thermocouples) while other techniques are capable of providing information on the temperature distribution (e.g. temperature distribution using PVD coatings of materials of known melting temperatures). The appropriate technique for temperature measurement depends on the application under consideration as well as the available tools for measurement.

Acknowledgements

This project was initiated by a grant from the NSF US–China co-operative research project on the Thermal Aspects of Manufacturing. One of the authors (R.K.) thanks Dr Alice Hogen of NSF for facilitating this activity and for her interest in this project. The authors are indebted to NSF for their continuing support to one of the authors (R.K.) at OSU on the various aspects of the manufacturing processes. Thanks are due, in particular, to Drs K. Narayanan, K. Rajurkar, Delci Durham of the Division of Design, Manufacturing, and Industrial Innovation (DMII) and to Dr Jorn Larsen Basse of the Tribology and Surface Engineering Program. One of the authors (R.K.) also thanks the A.H. Nelson, Jr. Endowed Chair in Engineering for support in the preparation of the paper. The authors also thank the reviewers for their valuable input which enhanced the quality of the paper.

References

[1] Kennedy FE. Surface temperatures in sliding systems — a finite element analysis. Trans ASME 1981;90:90–6.
[2] Komanduri R. Machining and grinding — a historical review of classical papers. Applied Mechanics Reviews 1993;46:80–132.
[3] Lenz E. Temperatures in metal cutting. In: International Conference on Manufacturing Technology. Dearborn, MI: ASTME, 1967:553–67.
[4] Barrow G. A review of experimental and theoretical techniques for assessing cutting temperatures. Annals of CIRP 1973;22(2):203–11.
[5] Kennedy FE. Surface temperature measurement. In: Blau PJ, editor. Friction, Lubrication, and Wear Technology. Metals Park, OH: ASM International, 1992:438–44.
[6] Thompson B. Count Rumford, an enquiry concerning the source of heat which is excited by friction. Phil Trans Royal Soc (Lon) 1798;18:278–87.
[7] Joule JP. On the mechanical equivalent of heat. Phil Trans of the Royal Soc (Lon) 1850;70:61–81.
[8] Taylor FW. On the art of cutting metals. Trans ASME 1906;28:31–248.
[9] Schmidt AO, Gilbert WW, Boston OW. A Thermal Balance Method and Mechanical Investigation of Evalutating Machinability, Trans ASME (1945) 225-232.
[10] Schmidt AO, Roubik JR. Distribution of heat generated in drilling. Trans ASME 1949;71:242–5.
[11] Sato K. Grinding temperature. Bull Jap Soc Grind Engrs 1961;1:3.
[12] Malkin S. Attritious and fracture wear. Sc.D. Thesis, MIT, 1968.
[13] Brecker JN. Ph.D. Thesis, Carnegie-Mellon University, Pittsburgh, PA, 1967.
[14] Hahn RS. The relationship between grinding conditions and thermal damage in the workpiece. Trans ASME 1956;78:807–10.
[15] Shaw MC. A new theory of grinding. Mech and Chem Engg Trans, Inst Eng (Australia) 1972;MC8(1):73–8.
[16] Komanduri R. Some aspects of machining with negative rake angles simulating grinding, Int. J. of Mach. Tool Des. Res. (1971) 223-233.
[17] Goldstein RJ, Chen PH, Chiang HD. Measurement of temperature and heat transfer. In: Rohsenow WM, Hartnett JP, Cho YI, editors. Handbook of Heat Transfer. New York: McGraw Hill Inc, 1998.
[18] Rall DL, Giedt WH. Heat transfer to, and temperature distribution in, a metal cutting tool. Trans ASME 1956;78:1507–15.
[19] Shaw MC, Pigott JD, Richardson LP. The effect of cutting fluids upon chip–tool interface temperatures. Trans ASME 1951;73:49–56.
[20] Kusters KJ. Das Temperaturfeld in Drehmeissel (The Temperatue Field in the Cutting Edge of a Cutting Tool). Essen, Germany: Verlag W. Girardet, 1954.
[21] Qureshi AH, Koenigsberger F. An investigation into the problem of measuring the temperature distribution on the rake face of a cutting tool. Annals of CIRP 1966;14:189–99.
[22] Shore H. Thermoelectric measurement of cutting tool temperatures. J Wash Acad Sci 1925;15:85–8.
[23] Gottwein K. Measurement of the temperatures in the turning of steels. Maschinenbau 1925;4:1129–35.
[24] Herbert EG. The measurement of cutting temperatures. Proc of the I Mech E (Lon) 1926;1:289–329.
[25] Trigger KJ. Progress report no. 1 on chip–tool interface temperatures. Trans ASME 1948;70:91–8.
[26] Trigger KJ. Progress report no. 2 on chip-tool interface temperatures. Trans ASME 1949;71:163–74.
[27] Shaw MC. Metal Cutting Principles. Oxford University Press, 1984.
[28] Outwater JO, Shaw MC. Surface temperatures in grinding. Trans ASME 1952;74:73–86.
[29] Bowden FP, Ridler KEW. The surface temperature of sliding metals. Proc of the Roy Soc (Lon) Ser A 1936;151:640–56.
[30] Spurr RT. Temperature reached by sliding thermocouples. Wear 1980;61:175–82.
[31] Blok H. Theoretical study of temperature rise at surfaces of actual contact under oiliness lubricated conditions. In: Proceedings of the General Discussion on Lubrication and Lubricants. London: Institute of Mechanical Engineers, 1938:222–35.
[32] Jaeger JC. Moving sources of heat and the temperature at sliding contacts. Proc Roy Soc of NSW 1942;76:203–24.
[33] Ling FF, Simkins TE. Measurement of pointwise junction condition of temperature at the interface of two bodies in sliding contact. Trans ASME, J Basic Engineering 1963;85:481–6.
[34] Furey MJ. Surface temperatures in sliding contact. ASLE Trans 1964;7:133–46.
[35] Dayson C. Surface temperature of unlubricated sliding contacts. ASLE Trans 1967;10:169–74.
[36] Tian X, Kennedy FE, Deacutis JJ, Hennig AK. The development and use of thin film thermocouples for contact temperature measurement. Tribology Trans 1992;35:491–9.
[37] Arndt G, Brown RH. On the temperature distribution in orthogonal machining. Int J Mach Tool Des Res 1967;7:39–53.
[38] Boothroyd G. Photographic techniques for the determination of metal cutting temperatures. Brit J of Appl Physics 1961;12:238–42.
[39] Boothroyd G. Temperatures in orthogonal metal cutting. Proc I Mech E (Lon) 1963;177:789–810.
[40] Jeelani S. Measurement of temperature distribution in machining using IR photography. Wear 1981;68:191–202.
[41] Schwerd F. Ueber die Bestimmung des Temperaturfeldes beim Spanablauf (Determination of the Temperature Distribution During Cutting). Z VDI 1933;9:211.
[42] Kraemer G. Neitrag zur Erkenntnis der beim Drehen auftretended Temperaturen und deren Messung mit einem Gesamtstrahlungsempfanger. Dissertation, Hannover, 1936.
[43] Mayer JE, Shaw MC. Grinding temperatures, Lubrication Engineering, J. of ASLE, (1957).
[44] Reichenbach GS. Experimental measurement of metal cutting temperature distribution. Trans ASME 1958;80:525.
[45] Chao BT, Li HL, Trigger KJ. An experimental measurement of metal cutting temperature distribution. Trans ASME 1961;83:496–504.

[46] Lenz E. Ein Beitrag zur Messung der schnittemperatur beim Drehen mit keramischen Schneidstoffen. Maschinenmarkt 1960;28:20.
[47] Lenz E. Der Einfluss der Schnittempertur auf die standzeit der keramischen Schneidstoffen. Maschinenmarkt 1963;28:30.
[48] Lenz E. Die Temperaturverteilung an der Spanunterseite in der Kontaktzone Span Wekzeug. Wekstattstechnik 1964;54:60.
[49] Lenz E. Die Temperaturverteilung in der Kontaktzone Span-Wekzeug beim Drehen von Stahl mit Hartmetall-Werkzeugen, Annals of CIRP, 14 (1966).
[50] Friedman MY, Lenz E. Determination of temperature field on upper chip surface. Annals of CIRP 1971;19:395–8.
[51] Prins OD. The influence of wear on the temperature distribution at the rake face. Annals of CIRP 1971;19:579–84.
[52] Ueda T, Hosokawa A, Yamamoto A. Studies on temperarature of abrasive grains in grinding — application of infrared radiation pyrometer. Trans ASME, J of Engg for Ind 1985;107:127–33.
[53] Ueda T, Hosokawa A, Yamamoto A. Measurement of grinding temperature using infrared radiation pyrometer with optical fiber. Trans ASME, J of Engg for Ind 1986;108:247–51.
[54] Ueda T, Yamada K, Sugita T. Measurement of grinding temperature of ceramics using infrared radiation pyrometer with optical fiber. Trans ASME, J of Engg for Ind 1992;114:317–22.
[55] Ueda T, Kanazawa K, Tanaka H, Torli A, Sugita T. Measurement of grinding temperature of active grains using infrared radiation pyrometer with optical fiber. Annals of CIRP 1993;42(1):405–8.
[56] Ueda T, Sato M, Nakayama K. The temperature of a single crystal diamond tool in turning. Annals of CIRP 1998;47(1):41–4.
[57] Bowden FP, Thomas PH. The surface temperature of sliding solids. Proc Roy Soc (Lon) A 1954;223:29–39.
[58] Parker RC, Marshall PR. The measurement of the temperature of sliding surfaces with particular reference to railway brake blocks. Proc of the I Mech E (Lon) 1948;158:209–29.
[59] Nagaraj HS, Sanborn DM, Winer WO. Direct surface temperature measurement by infrared radiation in eleastohydrodynamic contacts and the correlation with the Blok flash temperature theory. Wear 1978;49:43–59.
[60] Suzuki S, Kennedy FE. The detection of flash temperatures in a sliding contact by the method of tribo-induced thermoluminescence. Trans ASME, J of Tribology 1991;113:120–7.
[61] Schallbroach H, Lang M. Messung der Schnittemperatur mittels Temperaturanzeigender Farbanstriche. Zeitschrift des Vereines Deutscher Ingenieure 1943;87:15–9.
[62] Bickel E, Widmer W. Die Temperaturen an der Werkzeugschneide. Zurich, Switzerland: Industrielle Organization, 1954.
[63] Okushima K, Shimoda R. The cutting temperature. Bull of JSME 1957;23:73–7.
[64] Rossetto S, Koch U. An investigation of temperature distribution on tool flank surface. Annals of CIRP 1971;19:551–7.
[65] Kato S, Yamaguchi K, Watanabe Y, Hiraiwa Y. Measurement of temperature distribution within tool using powders of constant melting point. Trans ASME, J of Engg for Ind 1976;108:607–13.
[66] Kato T, Fujii H. PVD film method for measuring the temperature distribution in cutting tools. Trans ASME, J of Engg for Ind 1996;118:117–22.
[67] Wright PK, Trent EM. Metallographic methods of determining temperature gradients in cutting tools. J Iron and Steel Inst 1973;211:364–88.
[68] Trent EM, Wright PK. Metal Cutting. 4th ed Oxford, UK: Butterworth Heinemann, 2000.